Summer 8-23-2010

Optical Properties of In1-xGaxN Epilayers Grown by HPCVD

Jielei Wang Ms
Department of Physics and Astronomy Georgia State University

Optical Properties of $In_{1-x}Ga_xN$ epilayers grown by HPCVD

by

JIELEI WANG

Under the Direction of Nikolaus Dietz

ABSTRACT

Optical absorption spectroscopy has been applied to study properties such as the fundamental absorption edge and defect absorption centers of group III-nitride compound semiconductor epilayers. The investigation in this thesis focused on analyzing the band gap of indium-rich $In_{1-x}Ga_xN$ epilayers, which where grown by the high-pressure chemical vapor deposition (HPCVD) technique. Our results - together with literature data for gallium-rich $In_{1-x}Ga_xN$ alloys indicate that the shift of the fundamental band gap of $In_{1-x}Ga_xN$ with composition x can be described with a bowing parameter of b = 2.2eV. Temperature dependent transmission measurements show that the band gap variation with temperature follows a S-shape behavior for small gallium concentration and shifts towards a Varshni type behavior for a higher gallium concentrations. The S-shape behavior is attributed to nanoscale compositional fluctuations/clustering in the ternary alloy system. The thicknesses of the measured $In_{1-x}Ga_xN$ epilayers have been analyzed through multilayer stack model calculations of the transmission spectra. The free electron concentration in the $In_{1-x}Ga_xN$ epilayers has been obtained from simulations of infrared reflectance spectra.

INDEX WORDS: band gap, absorption, $In_{1-x}Ga_xN$, transmission, multilayer stack model, S-shape behavior

Optical Properties of $In_{1-x}Ga_xN$ epilayers grown by HPCVD

by

JIELEI WANG

A thesis Submitted in Partial Fulfillment of the Requirements for the Degree of

Master of Science

in the College of Arts and Sciences

Georgia State University

2010

Optical Properties of $In_{1-x}Ga_xN$ epilayers grown by HPCVD

by

JIELEI WANG

Committee Chair: Dr. Nikolaus Dietz

Committee: Dr. Unil A. G. Perera

Dr. Brian D. Thoms

Dr. Vadym Apalkov

Electronic Version Approved

Office of Graduate Studies

College of Arts and Sciences

Georgia State University

August 2010

To my parents Xiaonan, You and Chengxin, Wang

Acknowledgements

I would like to thank my advisor Dr. Dietz for letting me work in this research group and his patient guidance. I learned a lot during the last 2 years from him not only the research skills but also the ability to do things in an appropriate order. I would also like to thank my boyfriend Kun Huang for his support during the last 2 years. Last but not least, I would like to thank Dr. Perera, Dr. Thoms and Dr Apalkov for their advice and support during my research studies.

Table of contents

List of Tables

List of figures

Acronyms

Al	aluminum
CE	charge exchange
FIR	far infrared
Ga	gallium
HPCVD	High-pressure chemical vapor deposition
In	indium
IR	infrared
LED	light emitting diode
MBE	Molecular beam epitaxy
MDF	model dielectric function
MOVPE	Metalorganic vapor phase epitaxy
MQW	multiple quantum well
N	nitrogen
PL	photoluminescence
PMT	photomultiplier tube
SR	structural relaxation
VD	volume deformation

Chapter 1 Introduction

Group III-nitride compound semiconductor materials - e.g. AlInGaN alloys - have recently become one of the most interesting research topics due to their use in optoelectronic devices operating in the infrared, red, green, blue, violet and ultraviolet spectral wavelength regions. This wide spectral range enables a number of application including high-density data storage, high capacity DVD, high-resolution color printing, full color displays, as well as chemical and biological agent detection techniques. Next to the unique optical properties, group III-nitride semiconductors exhibit high thermal and chemical stability and have high electron mobilities, which allows their applications in high power transistors or field effect transistors.

During the last 30 years, significant progress in the material growth process and the development of GaN based optoelectronic devices. However, many fundamental physical properties of the III-nitrides are still unknown. Open questions concern relate for instance to the bulk, surface, and interface electronic properties. A very prominent uncertainty remains on the fundamental optical band gap of InN, which was up to the 90's assumed to be around 2 eV[1]. Experimental progress in the growth of InN by MBE[2,3] and MOVPE[4] indicate that the fundamental band gap is more likely around 0.7 eV[4,5], which led to renewed efforts to understand the fundamental physical properties of the group III-nitride material system.

The determination of optical properties and in particular of the dielectric function in the spectral range above the optical band gap (above the absorption edge) play an essential role for a better understanding of the materials properties. The energy position and relative amplitudes of specific absorption structures in the dielectric function are important parameter for improved band structure calculations. Together with complementary experimental data - for instance from Raman spectroscopy, infrared reflectance, atomic force microscopy, or transmission electron

microscopy - this investigation could contribute to a better microscopic understanding of the electronic properties. Furthermore, the measured optical properties are also a criterion for the crystal quality and/or the surface perfection. Whereas the band structure gives rise to certain absorption structures in the dielectric function of a material, the crystal quality typically leads to a reduction in the amplitude and an overall broadening of these structures.

The band gap value of $In_{1-x}Ga_xN$ alloys can be tuned from 0.65eV[6] to 3.42eV[7], covering the whole visible wavelength spectrum as illustrated in Figure 1.1. Though $In_{1-x}Ga_xN$ based multiple heterostructures with tailored compositions (values of x) are the basis for many optoelectronic devices such as LED or solar cells.

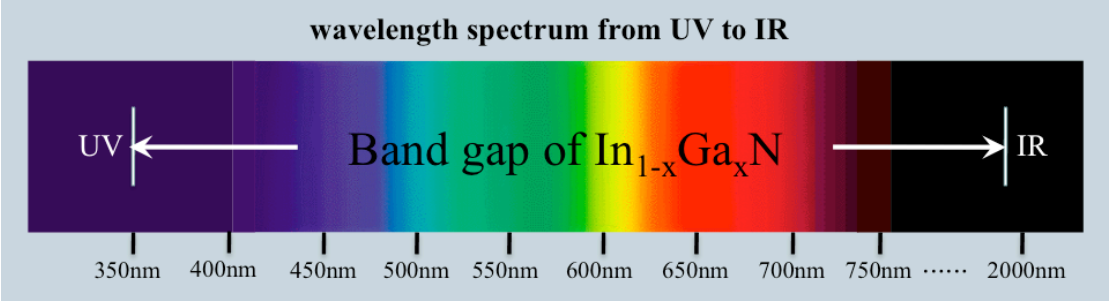

Figure 1.1 Band gap of $In_{1-x}Gax_xN$ as function of composition x, tuning from 0.7 eV to 3.5 eV.

Presently, the most challenging task in utilizing the full potential of group III-nitride alloys lays in the formation of ternary or quaternary group III-nitride alloys (e.g. InGaN, InAlN, or InAlGaN) at processing conditions that allows the integration of epilayers having different compositions. Theoretical predictions suggest that for $In_{1-x}Ga_xN$ in a composition regime of $0.15 < x < 0.85$ spinodal decomposition may occur, leading to indium-rich and gallium-rich $In_{1-x}Ga_xN$ regions or nano-clusters. However, local structure studies of InGaN did not show any evidence

for strong phase segregation, despite signs of a weak phase segregation being observed[8].

Under ambient conditions, two different crystal structures are known for group-III nitrides.[9] The thermodynamically stable phase is the hexagonal wurtzite structure. However, the cubic zincblende structure has been also stabilized by epitaxial layers. In both structures, the group-III atoms are coordinated by four nitrogen atoms and the other way around the nitrogen atoms are coordinated by four group-III atoms. The bonding geometry is determined by the sp^{3-} hybridisation of the common valence electrons. Thus, each atom is in particular also the center of a tetrahedron (see figure 1.2). These tetrahedrons arrange in planes, which consist of two interpenetrating hexagonal closest packed superlattices. The difference between both structures corresponds to the stacking sequence of the closest packed planes. While for the wurtzite structure the stacking sequence of these planes is ABABAB, the stacking sequence of the zincblende structure is ABCABC. The two stacking sequences are illustrated in figure 1.2.

In the following, we will focus on the wurtzite structure, since this is the only structure studied in this thesis. The wurtzite structure has a hexagonal unit cell, which contains six atoms of each element. Thus, two lattice constants 'c' and 'a' define the Bravais lattice. 'c' corresponds to the [0001] axis along the stacking direction of the hexagonal closest packed planes. 'a' is defined in the (0001) hexagonal closest packed planes and, thus, perpendicular to the c axis. Due to the 60° rotation symmetry in the hexagonal planes there exist three equivalent directions. These are the $[\bar{1}\,\bar{1}20]$, the $[\bar{1}2\bar{1}0]$, and the $[2\bar{1}\,\bar{1}0]$, which correspond to the lattice vectors $|a| \equiv |b| \equiv |c|$. At this point we would emphasize that the Miller indices for the wurtzite structure also contain 3 entries for all these directions perpendicular to the c axis and a fourth for the direction parallel to the c axis. In order to consider the redundance in this notation, the sum over the first three numbers has to be zero. The space group for the wurtzite structure is $P6_3mc$ (C_{6v}^4).[9]

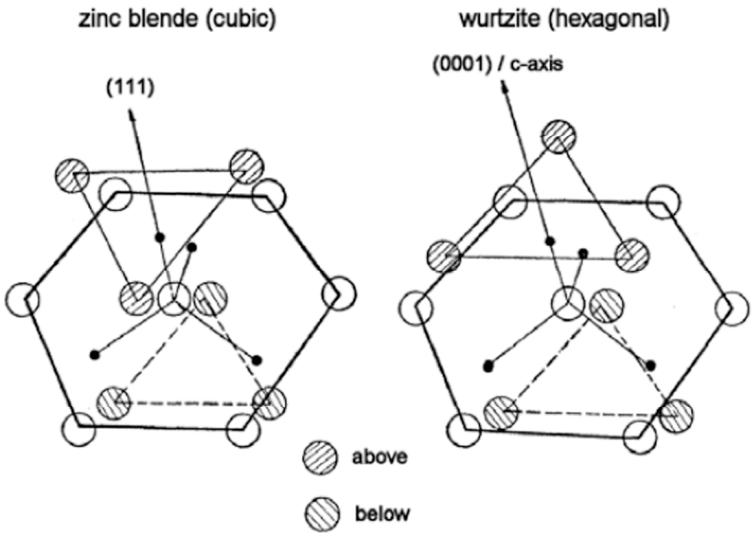

Figure 1.2: Schematic atomic arrangement of the first and second neighbors in the zinc blende and wurtzite crystal structure[9]. The large circles are group-III atoms and the small ones are N atoms. The two structures differ in only three of the twelve second neighbor atoms and even these are just rotated symmetrically by $\pi/3$.

In the wurtzite structure, the tetrahedrical chemical bonds are approximately aligned to the main crystal axis (planes). One of these four chemical bonds lies exactly parallel to the c-axis of the crystal, where as the other three approximately arrange in the hexagonal closest packed planes. If hexagonal crystal fields (polarization effects) are neglected, these bonds are tilted by about 19 deg against the hexagonal planes. In this ideal case of a undisturbed tetrahedrical chemical bond arrangement the c/a ratio of the lattice vectors should be 1.633. In real crystals the tetrahedrical chemical bond arrangement could be disturbed by through the crystal fields, which leads to variation on the c/a ratio.

The fact that the hexagonal wurtzite phase is the thermodynamically most stable structure, the wurtzite phase is also characterized as α-GaN, and α-InN, respectively (the cubic zincblende structure is denoted as β−phase). The room temperature lattice parameters for the α-

and β−phase of GaN and InN - together with the respective fundamental band gap energy - are summarized in Table 1.1.

	α-GaN	β-GaN	α-InN	β-InN
a [Å]	3.189	4.52	3.537	4.98
c [Å]	5.185	-	5.704	-
E_g [eV]	3.42	3.2 - 3.3	0.65 - 0.9 ?	?

Table 1.1: Lattice constants and fundamental band gaps of InN and GaN at room temperatures[10-12].

The further outline of this thesis is as follows:

In chapter 2, the experimental setup for the optical characterization of the thin film structures is described, including data acquisition and error analysis.

In chapter 3, the experiment result of the transmission and absorption spectra are presented for a selected number of $In_{1-x}Ga_xN$ epilayers grown with different composition x and varying process parameters such as V-III precursor ratio, or growth temperature.

Chapter 4 will provide a discussion of the experiment results and an outlook for further work.

1.1 Optical absorption spectroscopy

Absorption spectroscopy refers to spectroscopic techniques that measure the absorption of radiation, as a function of frequency or wavelength, due to its interaction with a sample. The sample absorbs energy, i.e., photons, from the radiating field. The intensity of the absorption varies as a function of frequency, and this variation is the absorption spectrum. Absorption spectroscopy is performed across the electromagnetic spectrum.

Absorption spectroscopy is employed as an analytical chemistry tool to determine the presence of a particular substance in a sample and, in many cases, to quantify the amount of the substance present. Infrared and ultraviolet-visible spectroscopic techniques are particularly common in analytical applications. Absorption spectroscopy is also employed in studies of molecular and atomic physics, astronomical spectroscopy and remote sensing.

There is a wide range of experimental approaches to measuring absorption spectra. The most common arrangement is to direct a generated beam of radiation at a sample and detect the intensity of the radiation that passes through it. The transmitted energy can be used to calculate the absorption. The source, sample arrangement and detection technique vary significantly depending on the frequency range and the purpose of the experiment.

Transmission spectroscopy

Transmission spectroscopy is related to Absorption Spectroscopy through the Beer Lambert's law. This technique can be used for solid liquid, and gas sampling. Transmission spectroscopy compares light passed through the sample with light entering the sample. The transmitted intensity depends on the sample thickness, absorption coefficient α of sample,

interfacial reflection coefficients, bulk and interface scattering, the angle of incident, crystal orientation, etc.

1.2 Beer-Lambert's Law

The Beer-Lambert's Law describes empirically the amplitude reduction of an electromagnetic (EM) wave due to absorption in a medium. Upon propagating a distance 'd' in the medium, the initial intensity I_1 of the EM wave will be reduced to

$$I_2 = I_1 \cdot e^{-\alpha(E)\cdot d}, \tag{1.1}$$

where $\alpha(E)$ is the absorption coefficient of the medium. Fig. 1.3 schematically illustrate light path. The initial intensity I_1 is related to the incoming intensity I_0 via $I_1=I_0(1-R)$, R, taking in account the reflectance at the ambient-medium interface.

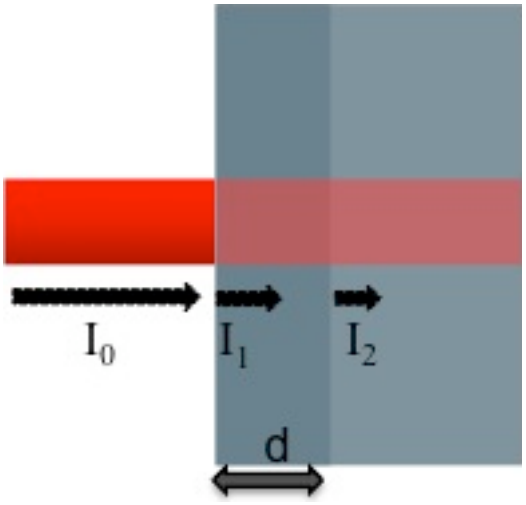

Figure 1.3 Beer-Lambert's Law.

1.3 Band gap shift as a function of the composition x of $In_{1-x}Ga_xN$

For many ternary semiconductor material such as $In_{1-x}Ga_xN$, $Al_{1-x}Ga_xN$, there is a correlation between the band gap value and the composition x. According to previous work and this work, it is shown that the correlation is not a linear behavior but a bowing behavior, which shows the band gap value is lower than that in a linear behavior.

There are three contribution to the bowing behavior[13].

1. Volume deformation (VD) term represent changes in the band gaps due to the compression of GaN and dilation of InN from their individual lattice constants to the alloy value a.
2. Charge exchange (CE) is calculated from the change in gaps bringing together GaN with InN forming $In_{1-x}Ga_xN$ with all atoms on unrelaxed zinc-blende lattice sites
3. Structural relaxation (SR) term represent changes in passing from the atomically unrelaxed to the relaxed alloy

In addition, doping and material defect structures can result in further inaccuracies in the analysis of bowing parameter. There are two types of absorptions for semiconductor: intrinsic and extrinsic. Intrinsic transitions refer to band-to-band absorption, excitonic absorption, free carrier absorption, inner shell electron absorption and phonon absorption. Band to band absorption is responsible for the fundamental absorption edge of the material since it is strong at and above the band edge region. Extrinsic absorptions take place either in the band edge region or FIR region. In the band edge region, valence band to donor, acceptor to conduction band and acceptor to donor transitions (as is shown in figure 1.4) are taking place.[23] So in the band edge

region, the extrinsic absorptions take place which causes the band gap value is lower than it is expected. And the acceptors and donors are mainly due to the doping or some defect structure. That's basically how the bowing behavior is coming from for the ternary semiconductor material.

The measured bowing parameters vary from 1 to 5 eV according to work reported in literature[14-20].

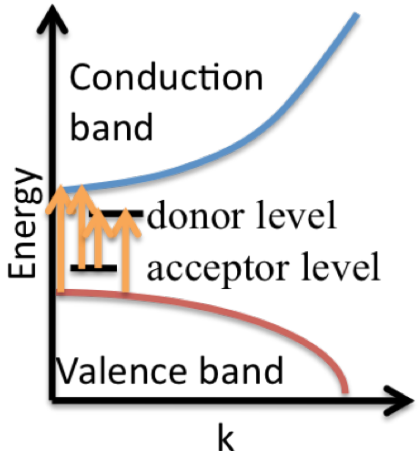

Figure 1.4 Electronic transitions for a direct semiconductor.

1.4 Band gap shift as function of temperature of $In_{1-x}Ga_xN$

It has also been reported that there is a temperature dependence of band gap of $In_{1-x}Ga_xN$. One is s-shaped behavior[21] which shows that the band gap drop, increase and again drop when the temperature is increasing. The other is Varshni behavior[22], which shows only a redshift of band gap when the temperature is increasing.

1.4.1 s-shape behavior

The mechanism of s-shaped behavior has been discussed in reference [21], based on photoluminescence (PL) measurements on InGaN/GaN multiple quantum wells (MQW's) and their and analysis. As depicted in Fig. 1.5, the temperature dependent PL spectra for typical InGaN/GaN MQW's show a 'S-shape' shift of peak position. The main emission peak shows an *S*-shaped shift with increasing temperature solid circles. The spectra are normalized and shifted in the vertical direction for clarity

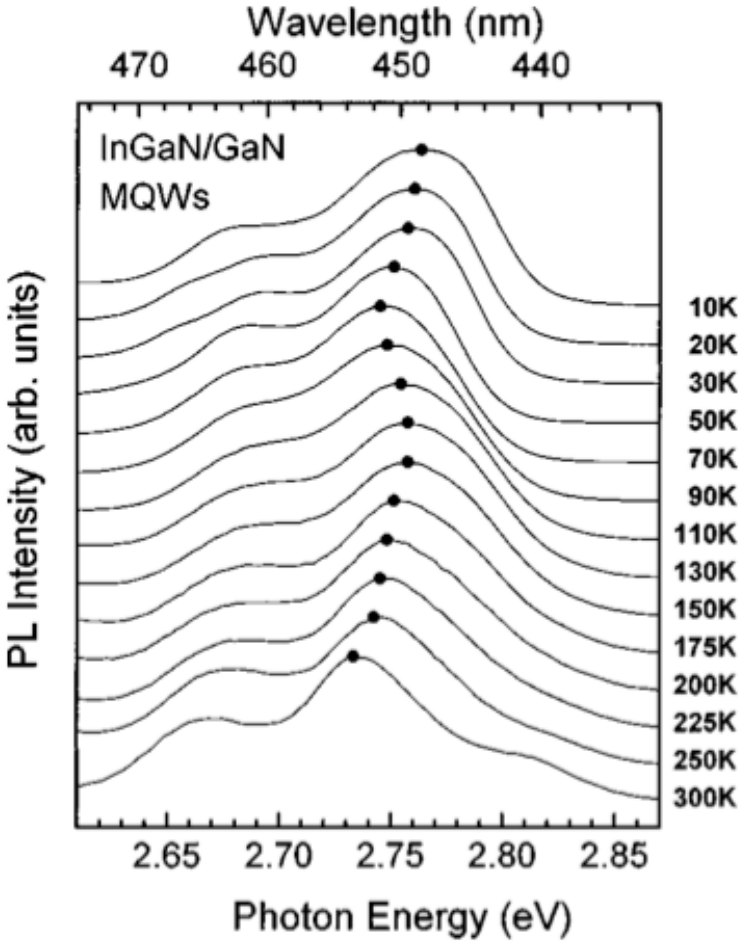

Figure 1.5 PL spectra for InGaN/GaN MQW's in the range from 10 - 300 K.[21]

This 'S-shape' behavior is is attributed to local potential variations and carrier

localization in the MQWs, a situation schematically illustrated in Fig. 1.6.

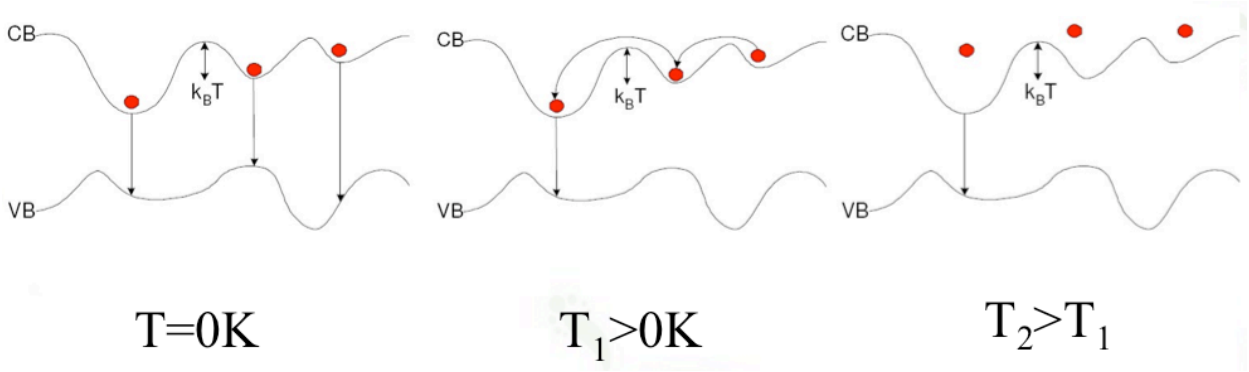

Figure 1.6 Schematic view of mechanism of S-shape behavior[23].

The effect of nanoscale inhomogeneities on the free carriers for the three temperature ranges is as followed:

(i) 10K < T < 70K range: Since radiative recombination processes are dominant, the free carrier lifetime increases. Potential fluctuations - due to nanoscale inhomogeneities / defects causes the recombining of the free carriers down in to lower energy tail states, which reduces the higher energy side emission and produces a redshift in the peak energy position with increasing temperature.

(ii) 70K < T < 150K range: The dissociation rate is increased and other nonradiative processes become dominant, the carrier lifetimes decrease with increasing temperature and are independent of the emission energies. Due to the decreased lifetime, these carriers recombine before reaching the lower energy tail states, leading to a blueshift in the peak energy.

(iii) For temperatures larger 150K, nonradiative recombination processes become dominant and the lifetimes are almost constant. The photo-generated free carriers are less affected by the fast change of carrier lifetime so the blueshift behavior becomes smaller. Hence the redshift prevails in this temperature range.

1.4.2 Varshni behavior

A typical temperature-dependent behavior of the PL peak position for undoped GaN can be described by a 'Varshni' behavior as shown in Fig. 1.7[24].

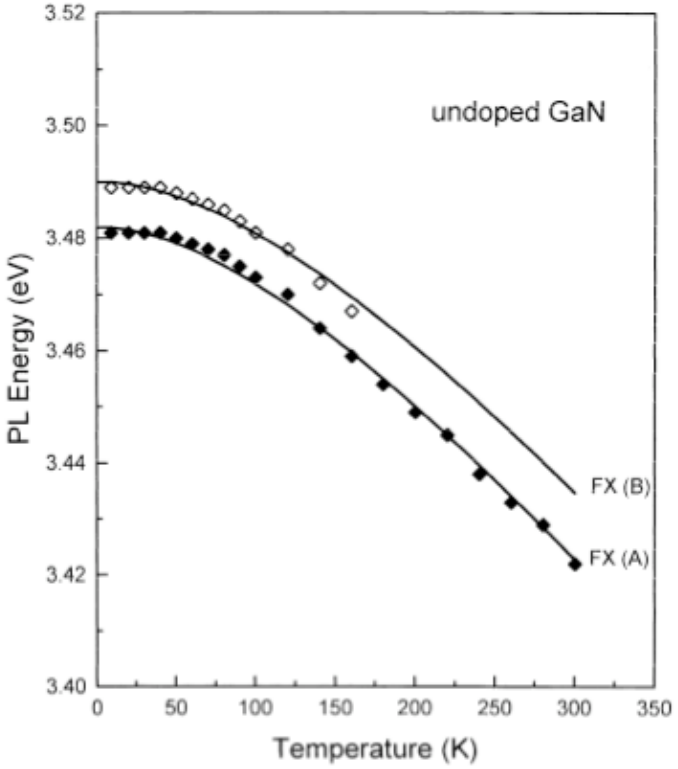

Figure 1.7 Varshni behavior of undoped GaN[24].

The Varshni relation[7] for the temperature dependence of semiconductor band gaps is

$$E_g(T) = E_0 - \alpha \cdot T^2 / (T + \beta) \tag{1.2}$$

In the Varshni equation, α and β are fitting parameters. And they are special for each type of material.

The mechanisms of Varshni behavior according to previous work are the following

two[22]:

1. The lattice constant will change when the temperature is changed[25,26] and theoretical calculations[26] show that the effect is linear with temperature at high temperatures. At low temperatures the thermal expansion coefficient is nonlinear with T.
2. The major contribution comes from a shift in the relative position of the conduction and valence bands due to a temperature-dependent electron lattice interaction. Theoretical treatments[16,27] show that this leads to a temperature dependence of the following form:

$$T << \theta: \quad \Delta Eg \propto T^2$$

and

$$T >> \theta: \quad \Delta Eg \propto T$$

where Θ is the Debye temperature.

1.5 Theory of Multilayer stack model

1.5.1 Dielectric function of Sapphire, InN, GaN, and $In_{1-x}Ga_xN$

Several models to approximate the dielectric function of InN and GaN have been reported in literature [28-30]. In this work, a modified 'model dielectric function' (MDF) approach taken from reference[27,31,32] has been used for GaN. This modified MDF approach describes best the anisotropic behavior of GaN and InN with hexagonal symmetry and perpendicular polarization. The data provided for InN are not correctly given and are adjusted as discussed in more detail below. Takeuchi et al.[33] used the same concept to establish the optical dielectric function for the ternary $Al_xGa_{1-x}N$ alloys system between its binaries GaN and AlN. The relative simple analytical expressions in the MDF approach provide a good agreement with experimental data.

The complex dielectric function as a function of energy E can be described by the sum of terms corresponding to one-electron contributions to four critical points (E_0, E_{1A}, E_{1B}, E_{1C}) as it is expressed in the following general formula

$$\varepsilon(E) = \varepsilon_0(E) + \varepsilon_{0x}(E) + \varepsilon_1(E) + \varepsilon_{1x}(E) + \varepsilon_\infty \qquad (1.3)$$

The dielectric functions $\varepsilon(E)$ of InN, GaN and $In_{1-x}Ga_xN$ can be parameterized via the critical points E_0 and $E_{1\beta}$ (with β=A, B, C). $\varepsilon_{0x}(E)$ and $\varepsilon_{1x}(E)$ are excitonic contributions at those critical points and E is the energy of the incident light.

Under the parabolic band assumption, the contribution of three-dimensional M_0 critical point E_0 is given by

$$\varepsilon_0(E) = AE_0^{-3/2}\chi_0^{-2}[2-(1+\chi_0)^{1/2}-(1-\chi_0)^{1/2}] \tag{1.5}$$

where $\chi_0 = \dfrac{E+i\Gamma_0}{E_0}$

A and Γ_0 are the oscillator strength and damping constants of the E_0 transition respectively.

The excitonic contributions at E_0 critical point are given by

$$\varepsilon_{0x}(E) = \sum_{m=1}^{\infty} \frac{A_0^{ex}}{m^3} \frac{1}{E_0 - (G_0^{3D}/m^2) - E - i\Gamma_0} \tag{1.6}$$

where A_0^{ex} is the three-dimensional (3D) exciton strength parameter and G_0^{3D} the 3D exciton binding energy

The contributions of the two-dimensional (2D) M_0 critical points $E_{1\beta}$ are given by

$$\varepsilon_1(E) = -\sum_{\beta=A,B,C} B_{1\beta}\chi_{1\beta}^{-2}\ln(1-\chi_{1\beta}^2) \tag{1.7}$$

$$\chi_{1\beta} = \frac{E+i\Gamma_{1\beta}}{E_{1\beta}} \tag{1.8}$$

with $B_{1\beta}$ and $\Gamma_{1\beta}$ are the strengths and damping constants of the $E_{1\beta}$ transitions, respectively.

The Wannier type 2D exciton contributions to the critical $E_{1\beta}$ points are given by

$$\varepsilon_{1X}(E) = \sum_{\beta=A,B,C}\sum_{m=1}^{\infty} \frac{B_{1\beta}^X}{(2m-1)^3} \frac{1}{E_{1\beta} - [G_{1\beta}^{2D}/(2m-1)^2] - E - i\Gamma_{1\beta}} \tag{1.9}$$

where $B_{1\beta}^{X}$ and $G_{1\beta}^{2D}$ are the strengths and the binding energies of the excitons at $E_{1\beta}$, respectively.

It has been shown that Gaussian broadening is a much better approximation for the broadening caused by electron-phonon and electron-impurities scattering. In this work, the damping constant Γ at critical point E_0 is replaced by the Γ' which is Gaussian broadening.

$$\Gamma'(E) = \Gamma \exp\left[-\alpha \left(\frac{E - E_g}{\Gamma} \right)^2 \right] \tag{1.10}$$

where α and Γ are adjustable model parameters, while E_g is the energy of the critical point at which transition occurs.

Additional oscillator around E_0 :

$$\varepsilon_{abi}(E) = \frac{S_{abi}}{E_{abi}^2 - E^2 - iE\Gamma_{abi}} \qquad i = 1,2,3 \tag{1.11}$$

where S_{abi}, E_{abi} and Γ_{abi} are the strength, energy position and damping constant of the oscillators, respectively.

Then the dielectric function is modified as

$$\varepsilon'(E) = \varepsilon(E) + \varepsilon_{ab1}(E) + \varepsilon_{ab2}(E) + \varepsilon_{ab3}(E) \tag{1.12}$$

Parameter	GaN	InN
ε_∞	0.426	1.500
A	41.251	3.000
Γ_0	0.287	0.300
α_0	1.241	1.241
E_0	3.550	0.700
B_{1A}	0.778	1.100
B_{1B}	0.103	0.700
B_{1C}	0.920	0.550
B_{1A}^X	2.042	1.042
B_{1B}^X	1.024	0.624
B_{1C}^X	1.997	1.400
Γ_{1A}	0.743	0.300
Γ_{1B}	0.428	0.380
Γ_{1C}	0.440	0.320
G_{1A}^{2D}	0.0003	0.0003
G_{1B}^{2D}	0.356	0.356
G_{1C}^{2D}	1.962	1.962
E_{1A}	6.010	5.350
E_{1B}	8.182	6.290
E_{1C}	8.761	6.750
A_0^{ex}	0.249	0.010
G_0^{3D}	0.030	0.020
Eab1	3.900	3.900
Sab1	0.000	29.00
Γab1	5.200	5.200
Eab2	7.900	7.900
Sab2	0.000	10.00
Γab2	0.600	0.600
Eab3	8.650	8.650
Sab3	0.000	17.00
Γab3	0.700	0.700

Table 1.2 Calculated parameters of GaN[27], InN(this work).

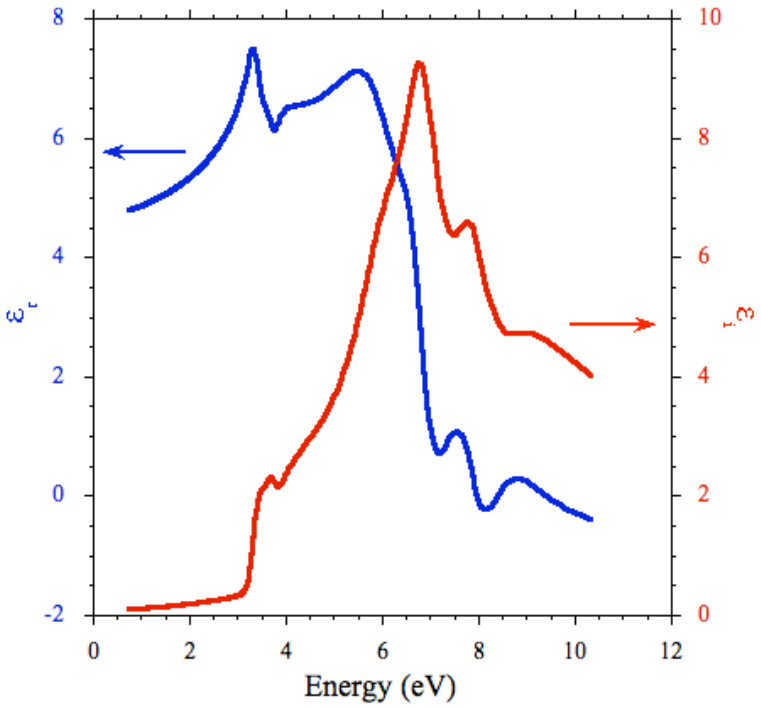

Figure 1.8 Imaginary part and real part of the dielectric function of GaN.

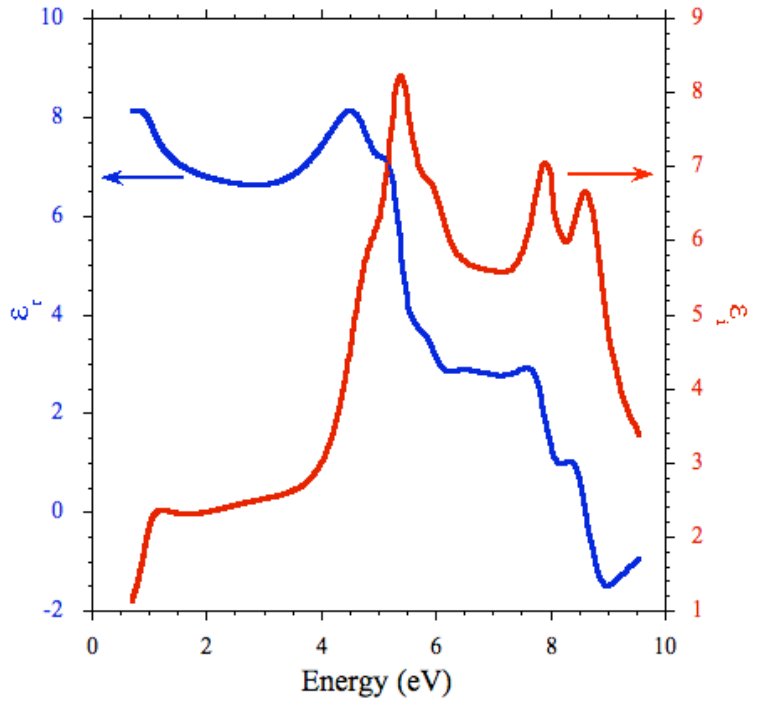

Figure 1.9 Imaginary part and real part of the dielectric function of InN.

The dielectric function of InN is constructed according to work[5]

To construct the dielectric function of $In_{1-x}Ga_xN$, the MDF oscillator equations are parameterized as function of composition x. The modified ε_{0x} oscillator for $In_{1-x}Ga_xN$ is given for example as:

$$\varepsilon_{0x}(h\omega, x) = \sum_{m=1}^{\infty} \frac{A_0^{ex}(x)}{m^3} \frac{1}{E_0(x) - [G_0^{3D}(x)/m^2] - h\omega - i\Gamma_0(x)} \tag{1.13}$$

where

$$\begin{aligned}
E_0(x) &= x \cdot E_0(\text{GaN}) + (1\text{-}x) \cdot E_0(\text{InN}) - b \cdot x \cdot (1\text{-}x) \\
A_0^{ex}(x) &= x \cdot A_0^{ex}(\text{GaN}) + (1\text{-}x) \cdot A_0^{ex}(\text{InN}) \\
G_0^{3D}(x) &= x \cdot G_0^{3D}(\text{GaN}) + (1\text{-}x) \cdot G_0^{3D}(\text{InN}) \\
\Gamma_0(x) &= x \cdot \Gamma_0(\text{GaN}) + (1\text{-}x) \cdot \Gamma_0(\text{InN})
\end{aligned}$$

b is the bowing parameter. Except the fundamental band gap value, all the other parameters for $In_{1-x}Ga_xN$ are constructed using the linear extrapolation. The $\varepsilon_1(x)$, $\varepsilon_{1x}(x)$, $\varepsilon_{abi}(x)$ and $\varepsilon_\infty(x)$ for $In_{1-x}Ga_xN$ are parameterized in the same way.

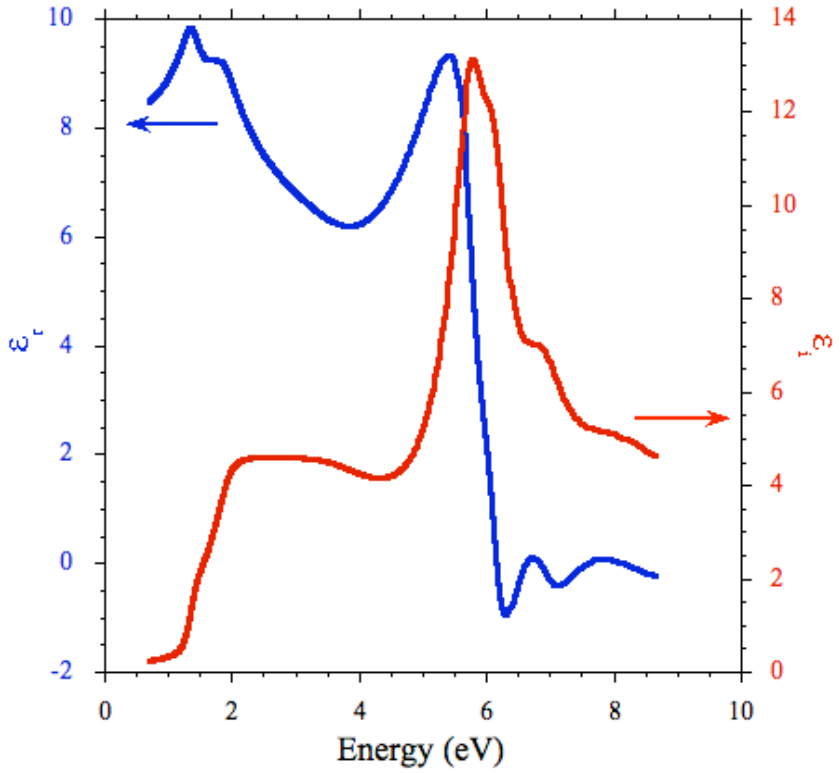

Figure 1.10 Dielectric function of $In_{1-x}Ga_xN$ with x=0.5

The dielectric function of sapphire is described by a Sellmeier equation expression[34] of form

$$\varepsilon_{sapphire} = 1 + \frac{A \cdot \lambda^2}{\lambda^2 - B} + \frac{C \cdot \lambda^2}{\lambda^2 - D} + \frac{E \cdot \lambda^2}{\lambda^2 - F} \tag{1.14}$$

with the Sellmeier coefficients A= 1.0237980, B= 0.0037759, C= 1.0582640, D= 0.0122544, E= 5.2807920, F= 321.36160.

1.5.2 Transmission and reflection in an multi-layered medium (Multilayer Stack theory)

The electromagnetic (EM) wave propagation at an interface between two media with different dielectric functions is given through the boundary conditions in the dynamic Maxwell Theory and subject of numerous publications.[35,36] In order to formulated the boundary conditions for the transmitted and incident EM wave is spilt with respect to the plane incidence into perpendicular and parallel field components. The reflection and transmission coefficients are analyzed with respect to these perpendicular and parallel field components.

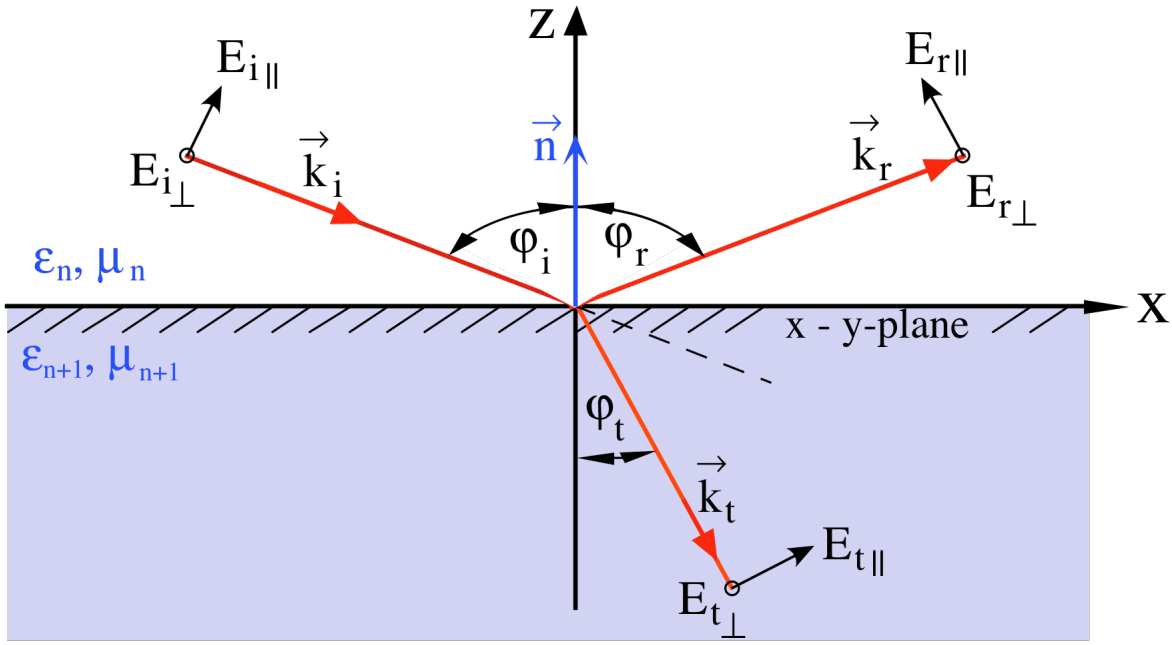

Figure 1.11: Schematic illustration of the incident, reflected and transmitted EM wave components with respect to the plane of incidence ($\vec{n}$) at an interface form by materials labeled as 'n' and 'n+1', with their dielectric functions ε_n and ε_{n+1}, respectively.

According to electrodynamic theory reflection and transmission coefficients are the following r_{pe} and t_{pe} are the coefficients when the electric field is perpendicular to the plane and r_{pa} and t_{pa} are the ones when the electric field is parallel to the plane. Now n is set to 1.

$$r_{pe} = \frac{Er}{Ei} = \frac{n_2 \cdot \cos\varphi_0 - \sqrt{n_2^2 - n_1^2 \cdot \sin^2\varphi_0}}{n_2 \cdot \cos\varphi_0 + \sqrt{n_2^2 - n_1^2 \cdot \sin^2\varphi_0}} \tag{1.15}$$

$$t_{pe} = \frac{Et}{Ei} = \frac{2n_1 \cdot \cos\varphi_0}{n_2 \cdot \cos\varphi_0 + \sqrt{n_2^2 - n_1^2 \cdot \sin^2\varphi_0}} \tag{1.16}$$

$$r_{pa} = \frac{Er}{Ei} = \frac{n_2^2 \cdot \cos\varphi_0 - n_1 \cdot \sqrt{n_2^2 - n_1^2 \cdot \sin^2\varphi_0}}{n_2^2 \cdot \cos\varphi_0 + n_1 \cdot \sqrt{n_2^2 - n_1^2 \cdot \sin^2\varphi_0}} \tag{1.17}$$

$$t_{pa} = \frac{Et}{Ei} = \frac{2n_1 \cdot n_2 \cdot \cos\varphi_0}{n_2^2 \cdot \cos\varphi_0 + n_1 \cdot \sqrt{n_2^2 - n_1^2 \cdot \sin^2\varphi_0}} \tag{1.18}$$

n in the equations above is the refraction index. When normal incident and with $n^2=\varepsilon$, reflection and transmission coefficient is simplified to equation 1.15 and 1.16

$$r = \frac{\sqrt{\varepsilon_2} - \sqrt{\varepsilon_1}}{\sqrt{\varepsilon_1} + \sqrt{\varepsilon_2}} \tag{1.19}$$

$$t = \frac{2 \cdot \sqrt{\varepsilon_1}}{\sqrt{\varepsilon_1} + \sqrt{\varepsilon_2}} \tag{1.20}$$

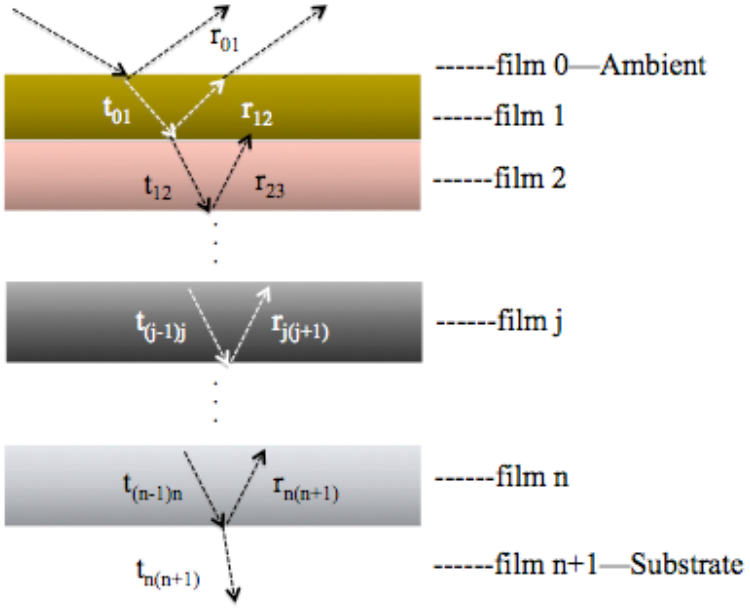

Figure 1.12 Multilayer stack.

Figure 1.12 depicts stratified structure that consists of a stack of 1, 2,...n parallel layers sandwiched between two semi-infinite ambient 0 and substrate n+1 media. r_{01}, r_{12}, r_{23}, $r_{n(n+1),}$ t_{01}, t_{12}, t_{23}, $t_{(n-1)n}$,$t_{n(n+1)}$ are the reflection and transmission coefficients at different interfaces of two films, respectively. For example, r_{23} is the reflection coefficient at the interface of film 2 and film 3. Let all media be linear homogeneous and isotropic and d_j and ε_j are the thickness and the dielectric function of the j^{th} layer, respectively.

Let $E^+(z)$ and $E^-(z)$ denote the complex amplitudes of the forward and backward traveling plane waves at an arbitrary plane z. So the total field at z can be described by:

$$E(z) = \begin{bmatrix} E^+(z) \\ E^-(z) \end{bmatrix} \tag{1.21}$$

Now we have two planes z' and z" parallel to the layer boundaries. Then E(z') and E(z") are correlated in a form:

$$E(z') = \begin{bmatrix} E^+(z') \\ E^-(z') \end{bmatrix} = \begin{bmatrix} S_{11} & S_{12} \\ S_{21} & S_{22} \end{bmatrix} \begin{bmatrix} E^+(z") \\ E^-(z") \end{bmatrix} = S \cdot E(z") \tag{1.22}$$

where

$$S = \begin{bmatrix} S_{11} & S_{12} \\ S_{21} & S_{22} \end{bmatrix} \tag{1.23}$$

We choose z' and z" to lie immediately on opposite sides of the j(j+1) interface. So between layers j and j+1 equation of E(z) becomes

$$E(z_{j+1} - 0) = I_{j(j+1)} E(z_{j+1} + 0) \tag{1.24}$$

where $I_{j(j+1)}$ is a 2 by 2 matrix, which describes the j(j+1) interface alone. Now if z' and z" are chosen inside the j^{th} layer at its boundaries, equation of E(z) becomes

$$E(z_j + 0) = L_j E(z_j + d_j - 0) \tag{1.25}$$

where L_j is another 2 by 2 matrix which describes the characteristic of the j^{th} layer alone whose thickness is d_i. For only the reflected wave in the ambient and the transmitted wave in the substrate can be detected, so it's necessary to relate their fields to those of incident and transmitted wave. By taking the planes z' and z" to lie in the ambient and substrate media, immediately adjacent to the 01 and n(n+1) interfaces respectively, equation of E(z) can be written in the form of:

$$E(z_1 - 0) = SE(z_{n+1} + 0) \tag{1.26}$$

in which S is a scattering matrix and it represents the overall reflection and transmission properties of the stratified structure. S can be expressed as a product of the interface and layer matrixes I and L as follows:

$$S = I_{01} L_1 I_{12} \cdots L_j I_{j(j+1)} \cdots L_n I_{n(n+1)} \tag{1.27}$$

According to the boundary condition, matrix I at the j(j+1) interface and L for the j^{th} layer can be obtained:

$$I_{j(j+1)} = \left(1 / t_{j(j+1)}\right)\begin{bmatrix} 1 & r_{j(j+1)} \\ r_{j(j+1)} & 1 \end{bmatrix} \tag{1.28}$$

$$L_j = \begin{bmatrix} e^{i\beta} & 0 \\ 0 & e^{-i\beta} \end{bmatrix} \tag{1.29}$$

where

$$\beta = \frac{2\pi d_j \sqrt{\varepsilon_j}}{\lambda} \tag{1.30}$$

β, d_j, ε_j are the phase factor, thickness and the dielectric function of the j^{th} layer, respectively.

So the overall scattering matrix S of the stratified structure can be found by matrix multiplication and equation of E(z) can be expanded as:

$$\begin{bmatrix} E(z_1^+ - 0) \\ E(z_1^- - 0) \end{bmatrix} = \begin{bmatrix} S_{11} & S_{12} \\ S_{21} & S_{22} \end{bmatrix}\begin{bmatrix} E(z_{n+1}^+) + 0 \\ 0 \end{bmatrix} \tag{1.31}$$

The overall reflection and transmission coefficients of the stratified structures are:

$$R = \frac{E(z_1^- - 0)}{E(z_1^+ - 0)} = \frac{S_{21}}{S_{11}} \tag{1.32}$$

$$T = \frac{E(z_{n+1}^+) + 0}{E(z_1^+ - 0)} = \frac{1}{S_{11}} \tag{1.33}$$

The scattering matrix for this system can be obtained as

$$S = \begin{bmatrix} S_{11} & S_{12} \\ S_{21} & S_{22} \end{bmatrix} = \left(\frac{e^{i(\beta_1+\beta_2+\cdots\beta_j+\cdots+\beta_n)}}{t_{01}\cdot t_{12}\cdots t_{j(j+1)}\cdots t_{n(n+1)}} \right) \bullet \begin{bmatrix} 1 & r_{01} \\ r_{01} & 1 \end{bmatrix} \bullet \begin{bmatrix} 1 & 0 \\ 0 & e^{-i2\beta_1} \end{bmatrix} \bullet \begin{bmatrix} 1 & r_{12} \\ r_{12} & 1 \end{bmatrix}$$

$$\cdots\cdots \bullet \begin{bmatrix} 1 & 0 \\ 0 & e^{-i2\beta_j} \end{bmatrix} \bullet \begin{bmatrix} 1 & r_{j(j+1)} \\ r_{j(j+1)} & 1 \end{bmatrix} \bullet \cdots\cdots \bullet \begin{bmatrix} 1 & 0 \\ 0 & e^{-i2\beta_n} \end{bmatrix} \bullet \begin{bmatrix} 1 & r_{n(n+1)} \\ r_{n(n+1)} & 1 \end{bmatrix}$$

(1.34)

Theoretical transmission then can be easily obtained by T=t·t*(when normal incident and t* is conjugate of t)

1.5.3 Calculation result and experimental result

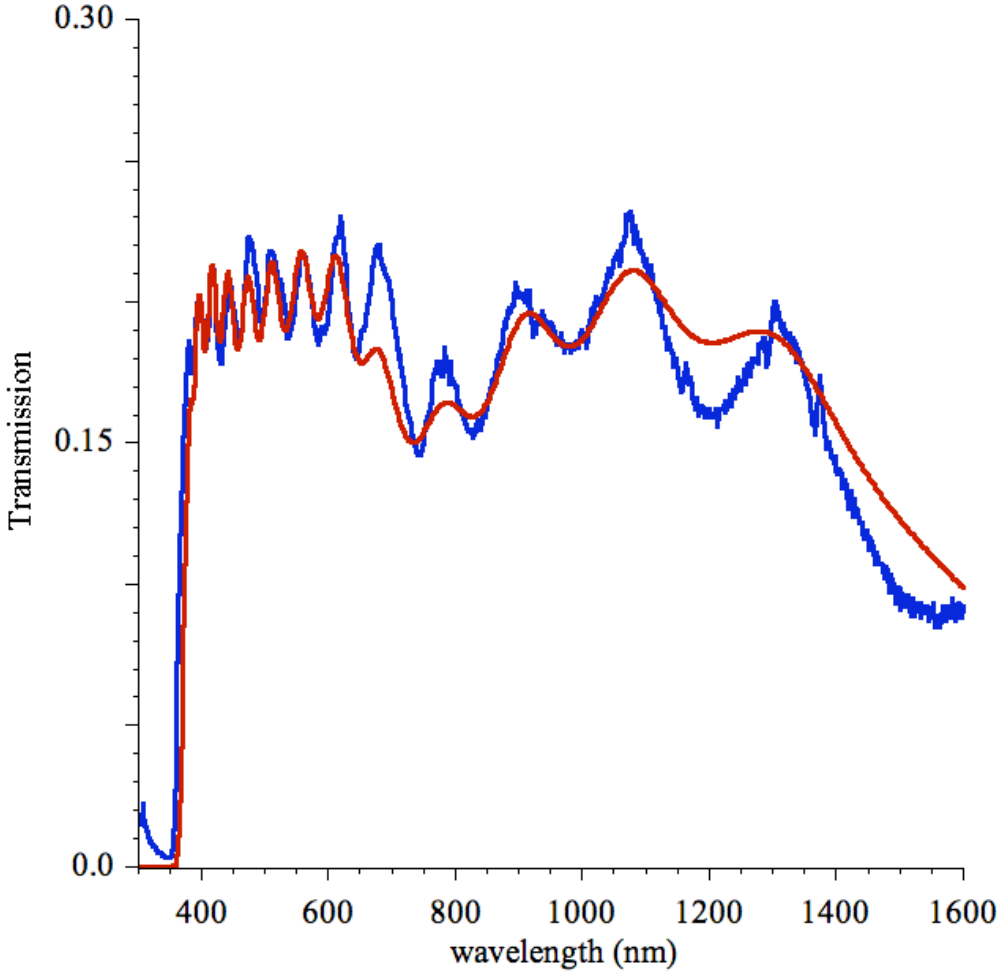

Figure 1.13 Calculation and comparison with experimental result of the GaN template of 509L.

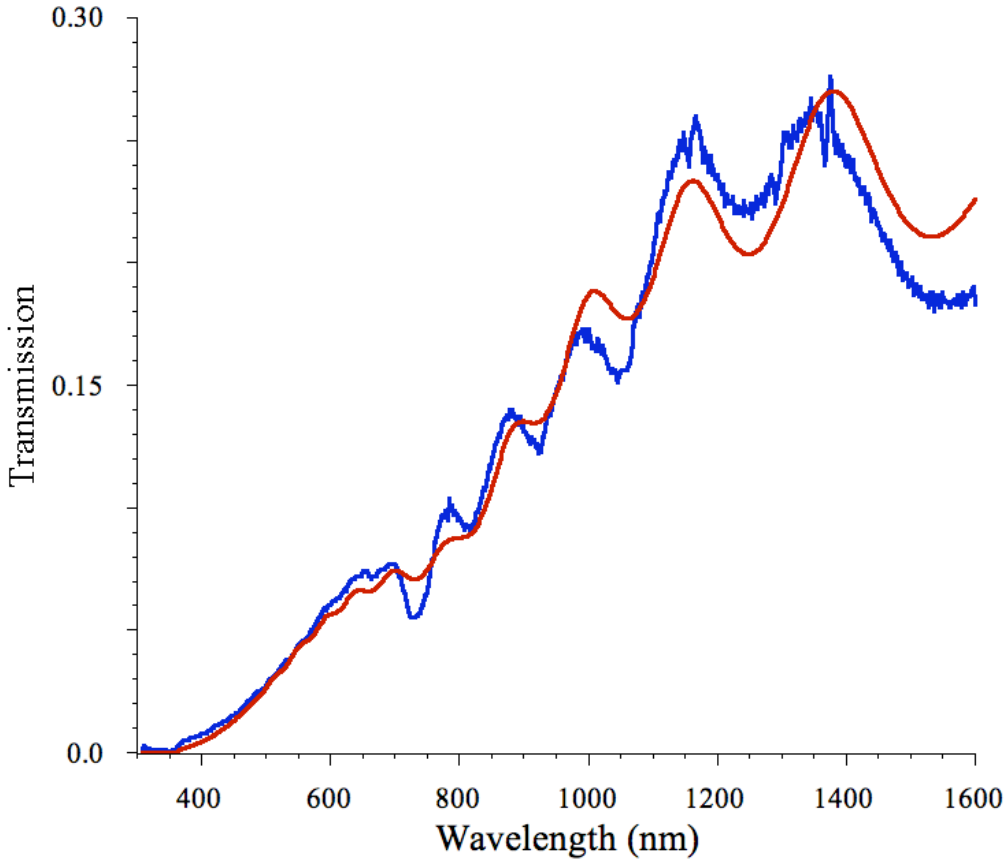

Figure 1.14 Calculation and comparison with experimental result 509L.

509L	ε_∞	thickness	Eg	x
GaN template	5.4	900nm	3.40eV	1.00
InGaN layer	5.0	190nm	2.02eV	0.67

Table 1.3 Calculation results for transmission spectrum from sample 509L.

Figure 1.13 and 1.14 show both the experimental and calculated results of transmission spectra of 509L GaN template and 509L sample. Red curves are the calculated curves and the blue ones are the experimental curves. The calculated result agrees well with the experimental

result including the interference fringes and the absorption edge. The detailed parameters, such as the film thicknesses d, additive constant ε_{∞}, band gap value Eg, and composition x are listed in table 1.3.

Chapter 2 Experimental setup

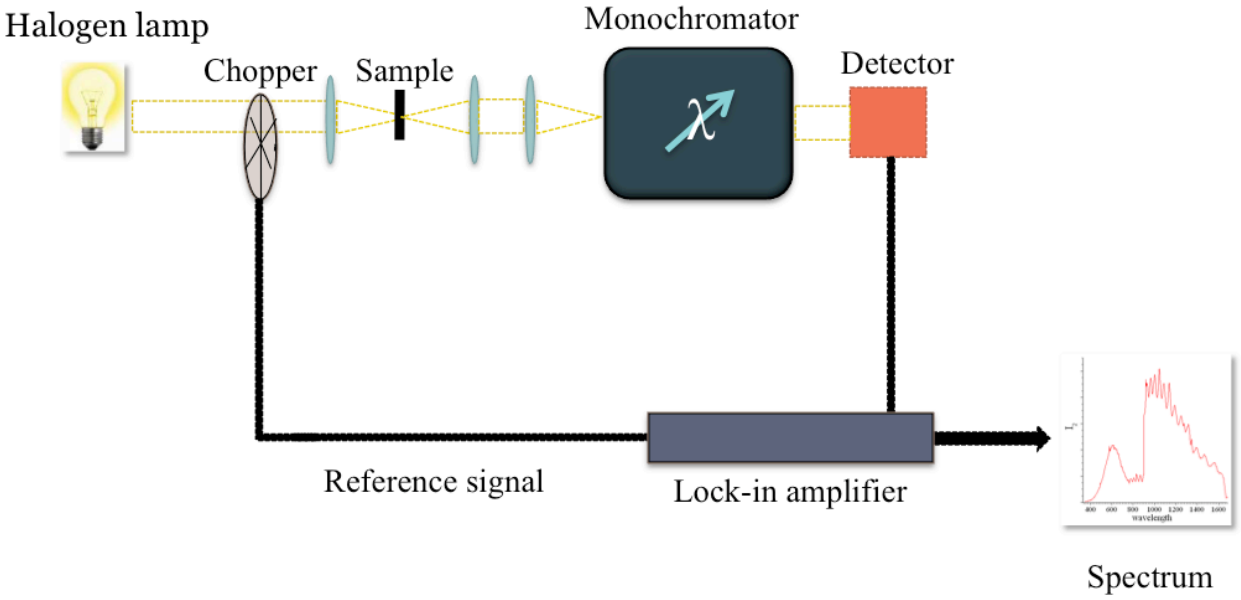

Figure 2.1 Experimental setup of room temperature transmission measurement.

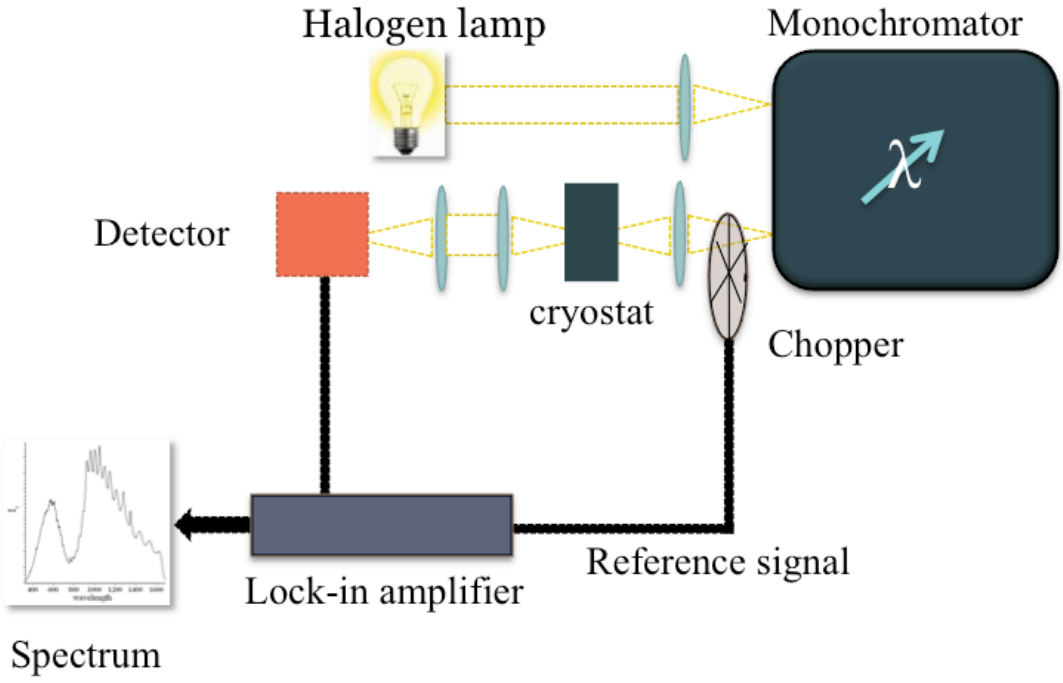

Figure 2.2 Experimental setup of temperature dependence transmission measurements.

Figure 2.1 depicts a schematic view of the experimental setup for transmission measurement. This setup is consist of a light source (Halogen lamp), lenses, an edge filter, a sample holder a monochromator, a detector and to reduce the noise level of the detector (PMT and InGaAs detector), a chopper and a lock-in amplifier.

In this thesis work, transmission measurements have been performed from 3.00eV to 0.75eV to observe the absorption properties of $In_{1-x}Ga_xN$. The samples are $In_{1-x}Ga_xN$ grown on GaN template which is the GaN grown on sapphire. Halogen lamp is used as light source and transmitted light is collected using photomultiplier tube (PMT) and Indium Gallium Arsenide (InGaAs) detector. Different filters are applied in different region. From 580nm to 850nm, OG550nm filter is used to block the second order of band edge of GaN.

Figure 2.2 depicts a schematic view of the experiment setup for temperature dependence transmission measurements. It's very similar to the room temperature transmission experiment setup. Halogen lamp is used as light source and PMT and InGaAs detector are used. What is different is that the monochromator was placed before the sample while in the former one the monochromator was placed after the sample. In this one, the temperature of the sample is varied from 4K to room temperature or higher using Helium flow and a heater. Experiments were done at the temperatures of 4K, 20K, 70K, 130K, 210K and 300K. In both experiments, the monochromator was used to select a certain wavelength. But the difference is in the first experiment, the monochromator selects the wavelength of light after the light comes out of the sample and in the second one the monochromator selects the wavelength before the sample. Sample 558L and 385L are measured with Ga percentage 15% and 10%, respectively. They are grown by HPCVD system and the parameters are listed in the next chapter

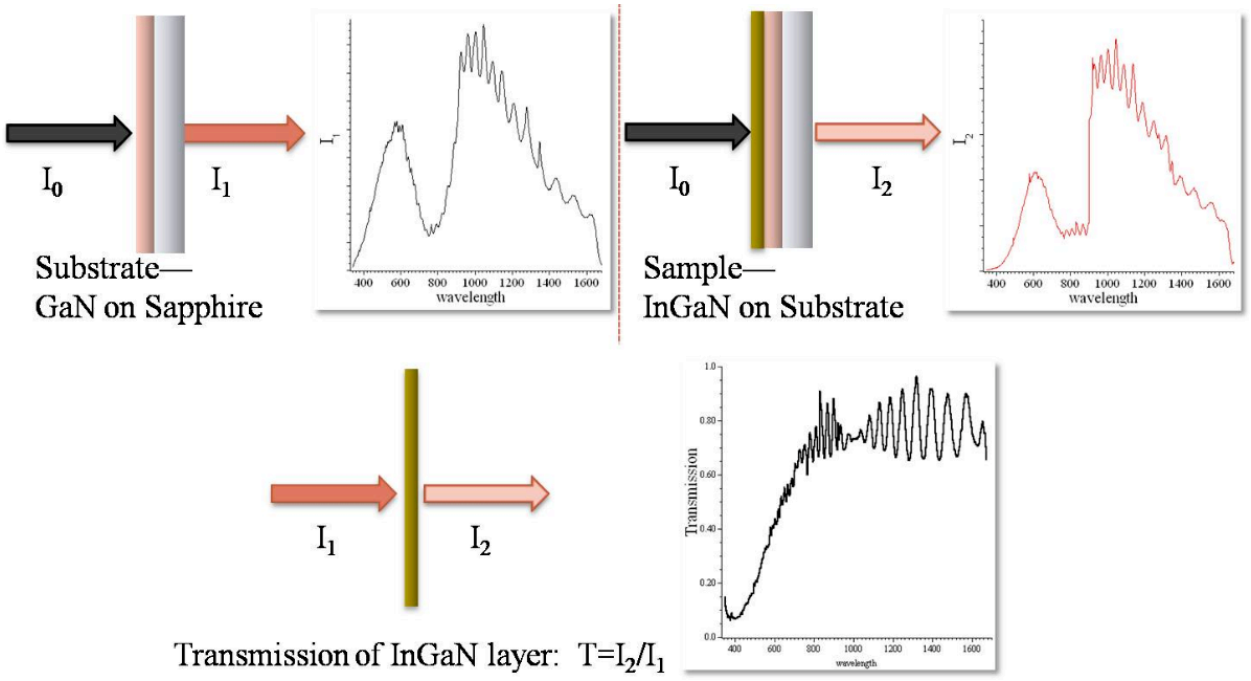

Figure 2.3: Experimental procedure to obtain the transmission spectrum of a InGaN layer

Figure 2.3 shows the experiment procedure for both experiments. First, the transmitted spectrum of the template (GaN grown on sapphire) is taken. And then the transmitted spectrum of the sample ($In_{1-x}Ga_xN$ grown on template) is taken. Since I_1 and I_2 can be written in the product of functions of the light source, monochromator, optical elements, detector and the transmission of $In_{1-x}Ga_xN$ and GaN layer:

$$I_1 = f_{lightsource} \bullet f_{monochromator} \bullet f_{elements} \bullet f_{detector} \bullet T_{template}$$

$$I_2 = f_{lightsource} \bullet f_{monochromator} \bullet f_{elements} \bullet f_{detector} \bullet T_{template} \bullet T_{InGaN}$$

So the transmission of the $In_{1-x}Ga_xN$ layer can be obtained by dividing I_1 by I_2.

Chapter 3 Results

3.1 Room temperature transmission measurement results of a set of $In_{1-x}Ga_xN$ samples

Sample #	Ga Composition x	Growth Temperature (^{0}C)	Reactor Pressure (bar)	V/III-ratio
440L	0.47	876	15.31	1250
443L	0.70	876	15.31	1253
449L	0.35	876	15.31	2025
509L	0.40	874	15.24	1462
557L	0.15	843	15.51	2998

Table 3.1 Growth parameters of a set of samples grown by High-pressure Chemical Vapor Deposition system.

Table 1 shows the set of $In_{1-x}Ga_xN$ samples grown by the High-pressure Chemical Vapor Deposition system with different compositions x which were analyzed in this work.

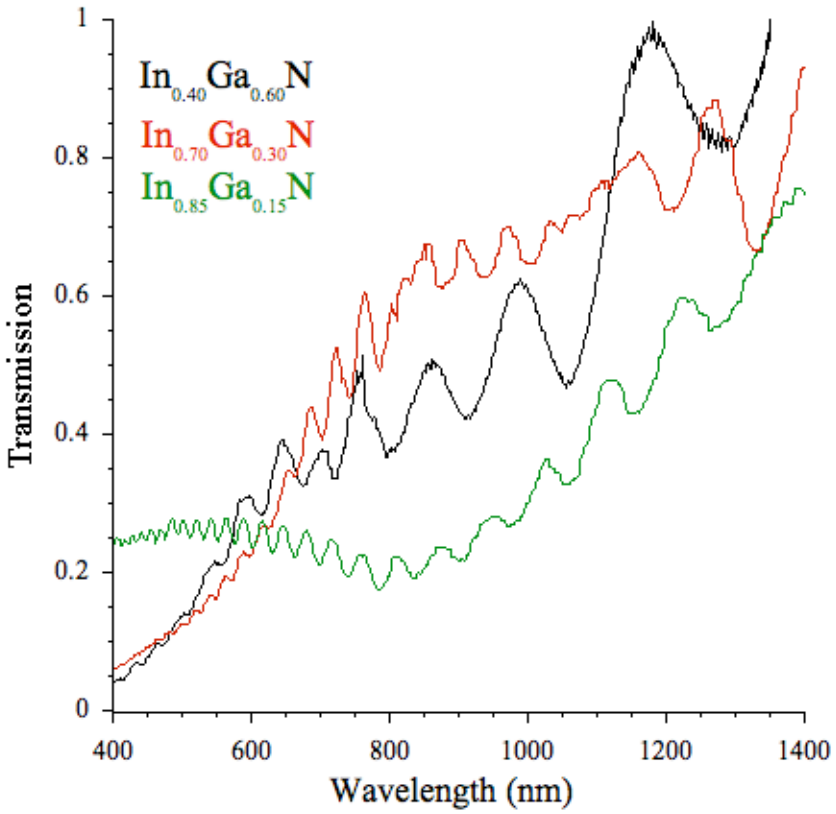

Figure 3.1 Transmission spectrum of $In_{1-x}Ga_xN$ with different Ga composition.

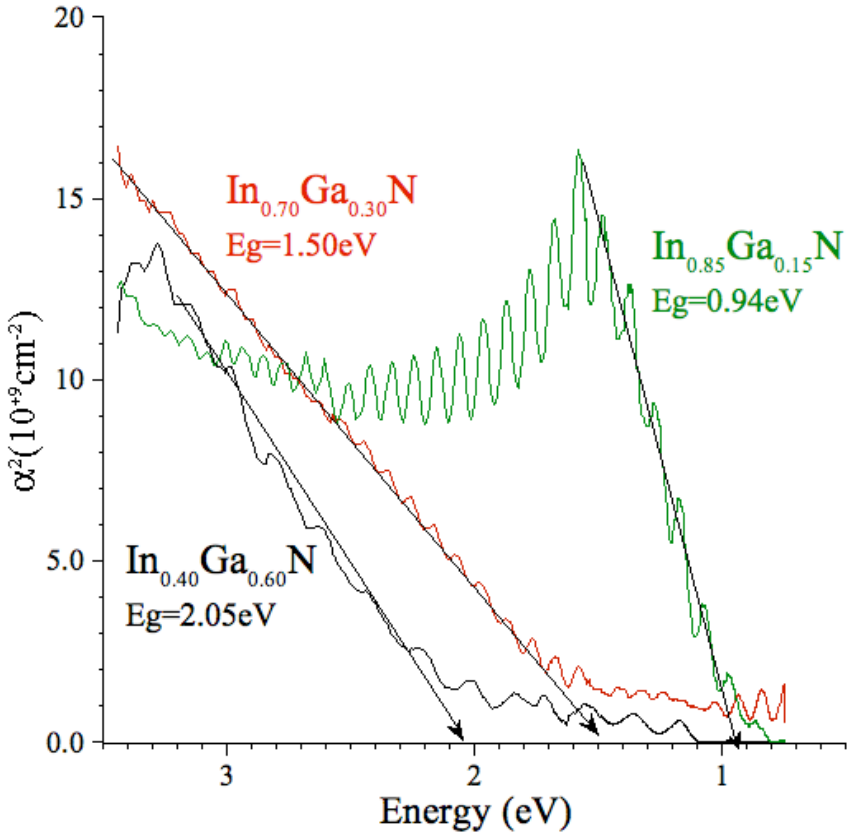

Figure 3.2 Absorption spectrum of $In_{1-x}Ga_xN$ with different Ga composition.

Figure 3.1 shows the transmission spectra of InGaN layers of three different gallium compositions. The absorption spectra in figure 3.2 were extracted from the transmission spectra using the Beer Lambert's law. In figure 3.2 the interception of the slope of the absorption curve and the energy axis is the band gap value. Linear fit to the slope of the curve is used to get the band edge of the material from the interception of the slope and the energy axis.

x	0	0.15±0.11	0.30±0.08	0.47±0.13	0.60±0.06	0.70±0.05	1
Eg[ev]	0.65	0.94±0.11	1.50±0.35	1.35±0.09	2.05±0.12	2.38±0.02	3.42

Table 3.2. Band gap values of different $In_{1-x}Ga_xN$ with different x.

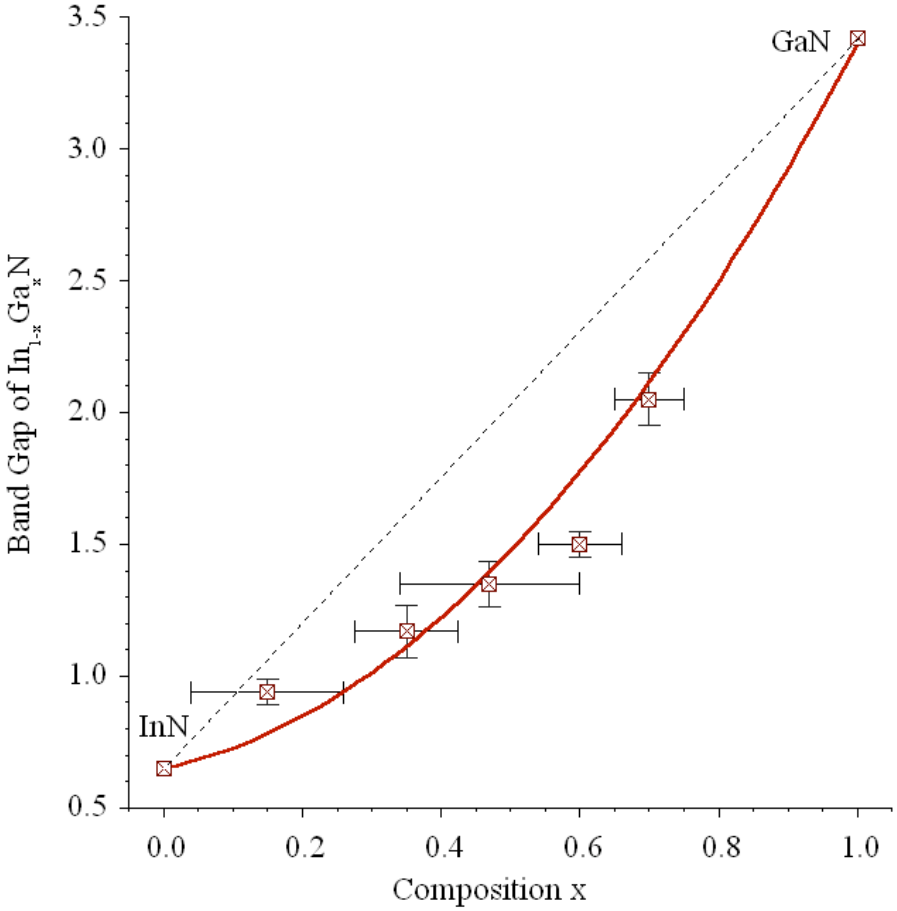

Figure 3.3 Band gap value vs. Ga composition x.

Table 3.2 lists the values of the band gap energy determined for various compositions.

Figure 3.3 is a graph of the band gap value against the composition x and from which we can see the correlation between band gap value and composition x is not a linear but a bowing behavior. The red squares are the experimental data and the red curve is the fitting of the bowing behavior using the formula below. Hence the band gap value of $In_{1-x}Ga_xN$ can be calculated in the form of the following formula where a bowing parameter is applied here:

$$E_g = x \cdot E_g^{GaN} + (1-x) \cdot E_g^{InN} - b \cdot x \cdot (1-x) \tag{3.1}$$

The bowing parameter calculated here is 2.2±0.1eV, which is somewhat higher than the recent reported bowing parameter of 1.6 eV by Goldhahn et al.[37]. As mentioned in the first chapter, there are large variations in the reported values of the bowing parameter due to the lack of sufficient good InGaN alloys. Since the bowing parameter is affected by the strucutrual layer quality, the defect density and types of defects in the alloys, as well as the doping level, the reported values of the bowing parameter depends strongly by the growth methods used and even from the growth facility.

3.2 Temperature dependence of the band gap of $In_{1-x}Ga_xN$

Table 3.3 summarizes the growth parameter/conditions of the InGaN epilayers analyzed by temperature-dependant absorption spectroscopy. These measurements were performed to study the fundamental band gap shift as function of temperature and how potential crystal imperfections affect this shift.

Sample #	Ga Composition x	Growth Temperature (^{0}C)	Reactor Pressure (bar)	V/III-ratio
385L	0.10	876	9.25	1122
558L	0.15	837	15.51	2998

Table 3.3 Growth parameters of the samples for the temperature dependent measurements.

Figure 3.4 depict the transmission spectra of the $In_{0.85}Ga_{0.15}N$/GaN/Sapphire structure (sample # 558L) measured from 4K up to 300K. The computed absorption spectra of sample 558L are show in Figure 3.5 for the temperatures of 4K, 20K, 70K, 130K, 210K and 300K. The

absorption spectra are plotted in terms of alfa^2 over energy, which allows to estimate the band gap values from a linear slope fit of the spectra and its intercept with the energy x-axis. The estimated band gap values as function the temperature are shown in the inset in Fig. 3.5. The analysis shows that the band gap values decrease with increasing temperature, following a Varshni type behavior.

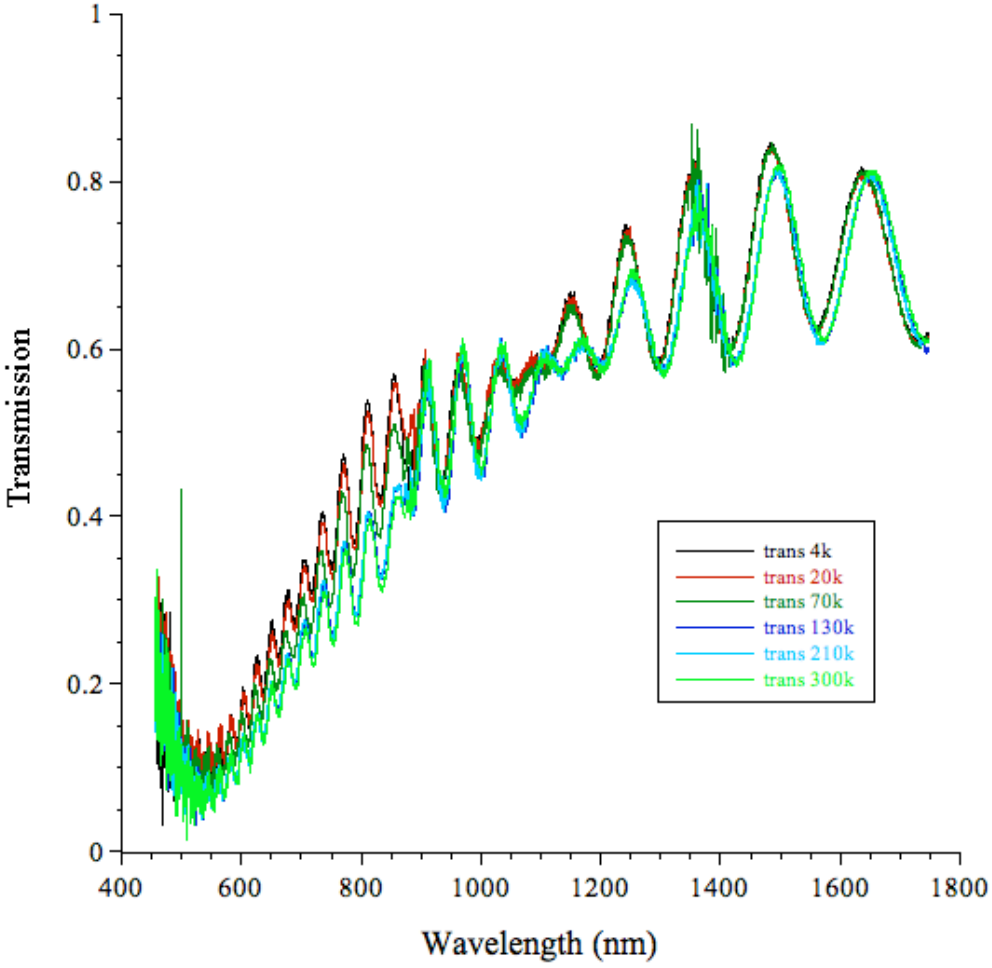

Figure 3.4 Transmission spectra of sample 558L $In_{0.85}Ga_{0.15}N$ for different temperatures.

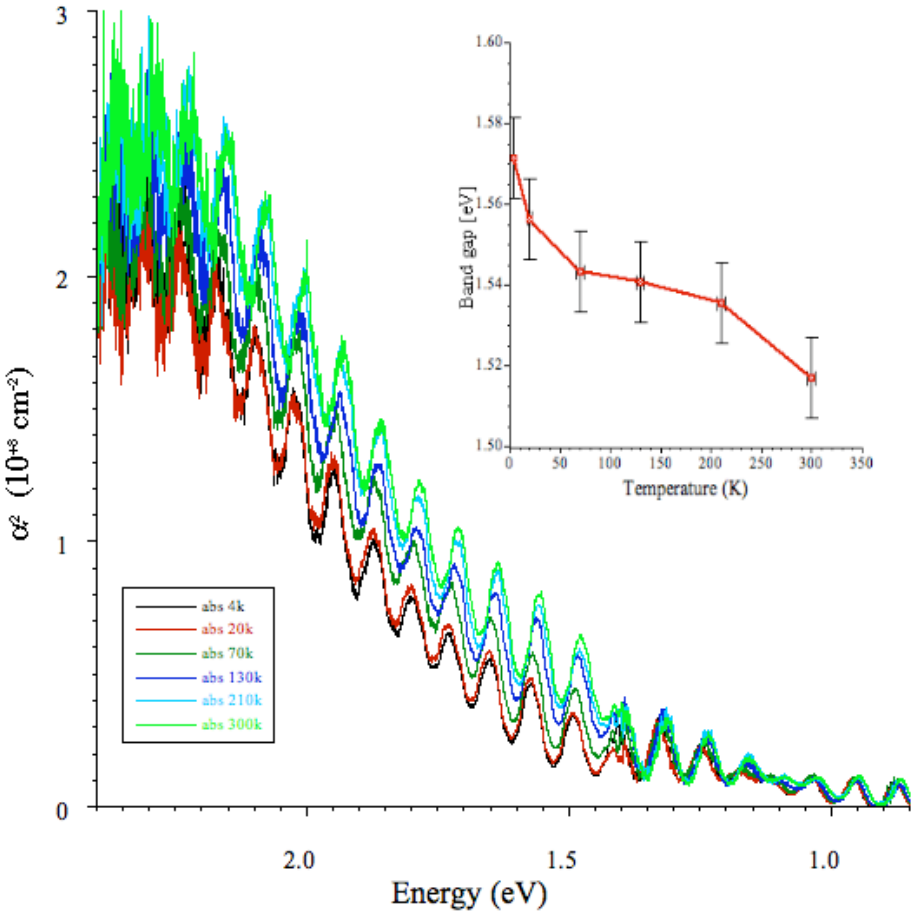

Figure 3.5 Temperature dependence of absorption spectra and the relation between the band gap value and the temperature of sample 558L $In_{0.85}Ga_{0.15}N$.

Figure 3.6 depict the transmission spectra of the $In_{0.9}Ga_{0.1}N$/GaN/Sapphire structure (sample # 385L) measured from 4K up to 300K. The calculated absorption spectra of sample 385L are show in Figure 3.7 for the temperatures of 4K, 20K, 70K, 130K, 210K and 300K. As before, the band gap values as function of temperature as estimated from a linear slope fit from the alfa^2 over energy plot and its intercept with the energy x-axis. The analyzed band gap values are depicted in the inset in Fig. 3.7, showing a 'S-shape' type of behavior with increasing temperature.

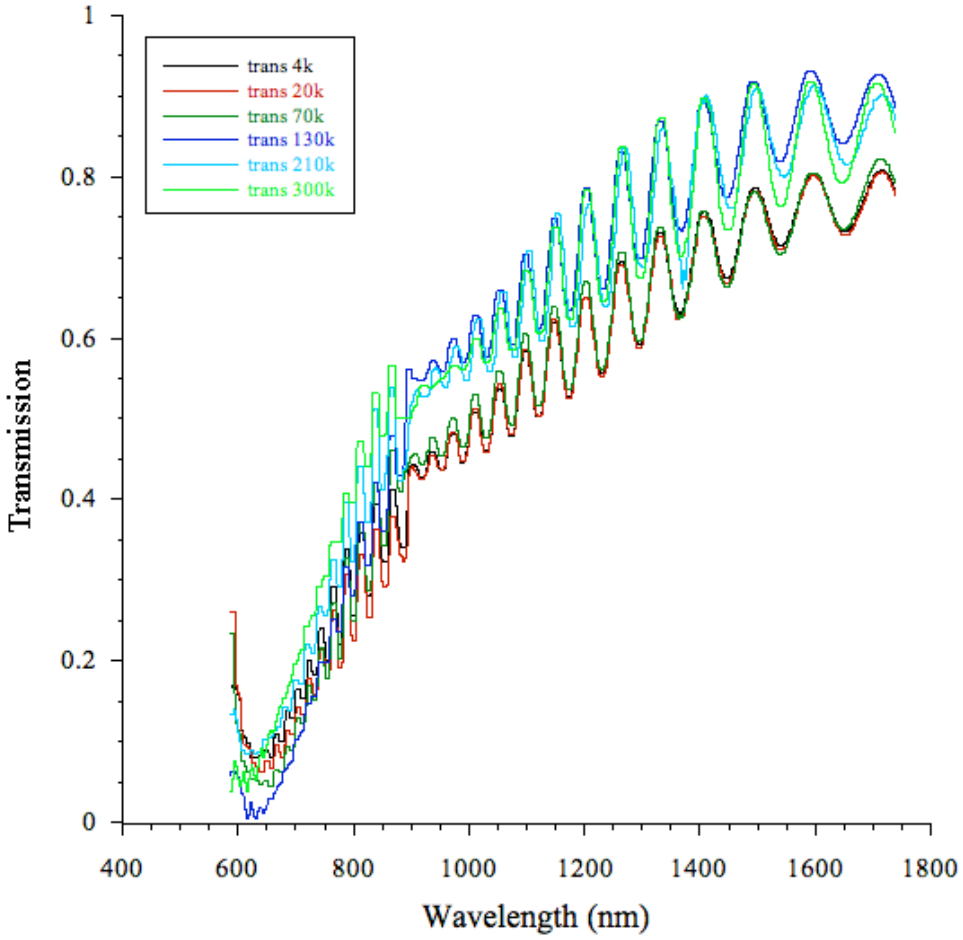

Figure 3.6 Transmission spectra of sample 385L $In_{0.9}Ga_{0.1}N$.

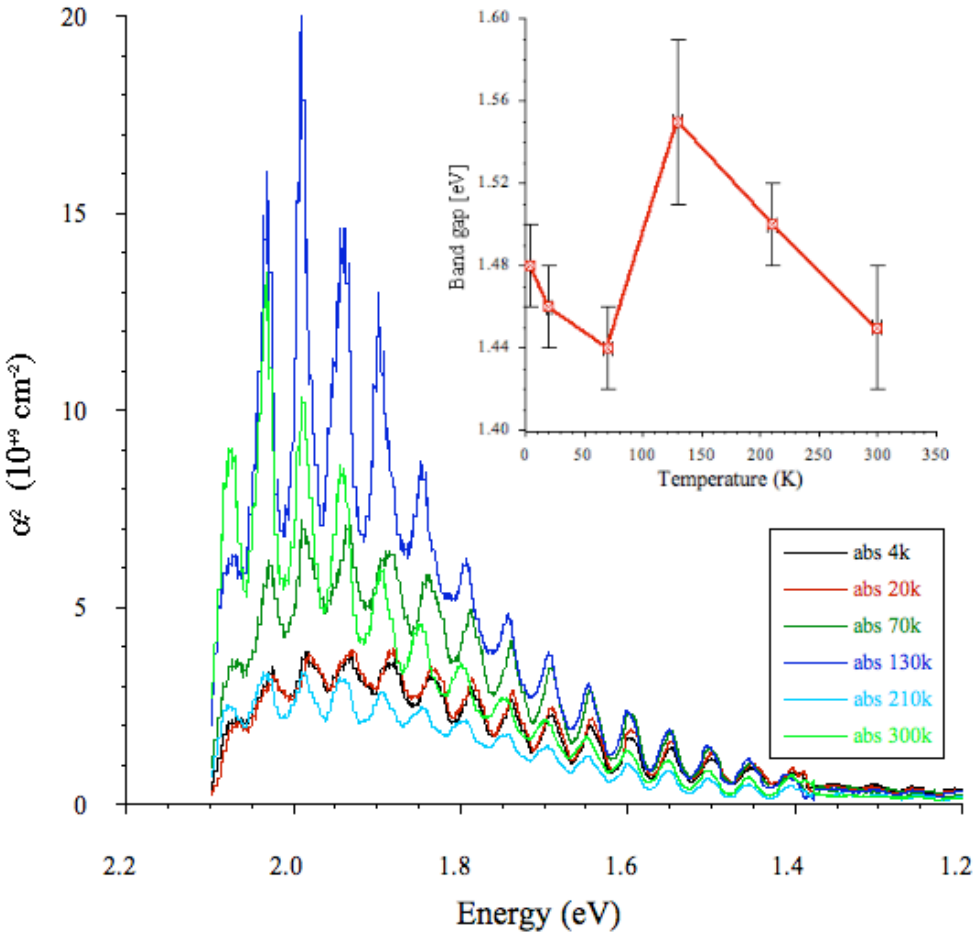

Figure 3.7 Temperature dependence of absorption spectra and the relation between the band gap value and the temperature of sample 385L $In_{0.9}Ga_{0.1}N$.

Chapter 4 Discussion

Figure 3.1 depicts the room temperature transmission spectra of $In_{1-x}Ga_xN$ with different Ga compositions. The amplitudes of the transmission spectra vary due to different surface and interfacial roughnesses in the different samples, which affects the scattering coefficients of the surface and the interfaces between the multilayer stack. These interfacial imperfections also affect the reflectance amplitudes on each interface, reducing the overall transmission and reflectance values observed. As mentioned in the first chapter, the interfacial scattering affects the transmission and causes different maximum amplitude of transmission for different samples. Since these are interfacial effects, the estimated absorption edge of th InGaN should be not directly affected.

Figure 3.2 shows the absorption spectra of $In_{1-x}Ga_xN$ layers with various Ga composition. The spectra were derived from the transmission spectra using Beer Lamberts Law given in chapter 1. The figure shows clearly the different slopes for the absorption edges for the various Ga compositions. The band gap values are estimated from the slope intercept with the energy x-axis. The estimated fundamental band gap values are plotted as a function of composition x of $In_{1-x}Ga_xN$ in figure 3.3, showing a nonlinear behavior for the band gap value with Ga composition x. The values are lower than in a linear correlation, requiring a negative bowing parameter for the correct description. At present, the exact origin and other contributions to the bowing parameter are not knows. As indicated in chapter one, structural and point defects dopants, and doping levels may strongly affect the fundamental absorption edge and with it the

estimated band gap values. These contributions might explain an overestimate of the bowing parameter, which was estimated in this work to 2.2±0.1eV.

Figure 3.4 and 3.6 show the transmission spectra for the temperature dependent measurements of the InGaN samples 558L and 385L, respectively. As shown in these two figures, the minimum transmission values are not zero in the high-energetic region, which is due to the detector noise limitation. These regions in the spectra were excluded from the analysis of the absorption spectra, which are shown in figures 3.5 and 3.7, respectively.

Figure 3.5 depicts the evolution of the absorption edge for sample 558L $In_{0.85}Ga_{0.15}N$ over a temperature range from 4 to 300K. It shows that the band gap decreases with increasing temperatures, which overall form is described by a Varshni-type behavior.

However, a care analysis shows that form is composed of an Varshni-type behavior with and super-imposed s-shape behavior. From 4 to 70K, the band edge is redshifted by 40meV. From 70 to 210K, the band edge is only redshifted by 5meV, and from 210 to 300K, it is again redshifted 25meV. If a linear backgroup is subtracted from the curve, an s-shape behavior is observed. So, both varshni and s-shape behavior exist from the result of this experiment for sample 558L.

Figure 3.7 depicts how the gap changes when the temperature is changed for sample 385L $In_{0.9}Ga_{0.1}N$. It shows that the band gap value decreases 37meV from 4K-70K, and in the range of 70K-130K, the band gap values increases for 110meV. When the temperature is further increased from 130K, the band gap value decreases 97meV. An s-shape behavior is clearly seen in the analysis of this measurement.

References:

[1] T.L. Tansley and C.P. Foley, "Optical band gap of indium nitride," J. Appl. Phys. **59**(9) pp. 3241-4 (1986).

[2] T. Inushima, V. V. Mamutin, V. A. Vekshin, S. V. Ivanov, T. Sakon, M. Motokawa, and S. Ohoya, "Physical properties of InN with the band gap energy of 1.1 eV", J. Cryst. Growth **227-228** pp. 481-485 (2001).

[3] J. Wu, W. Walukiewicz, K. M. Yu, J.W. A.III, E. E. Haller, H. Lu, W.J. Schaff, Y. Saito, and Y. Nanishi, "Unusual properties of the fundamental band gap of InN", Appl. Phys. Lett. **80**(21) pp. 3967-3969 (2002).

[4] T. Matsuoka, H. Okamoto, M. Nakao, H. Harima, E. Kurimoto, "Optical bandgap energy of wurtzite InN", Appl. Phys. Lett. **81**(7), 1246-1248 (2002).

[5] R. Goldhahn, A. T. Winzer, V. Cimalla, O. Ambacher, C. Cobet, W. Richter, N. Esser, J. Furthm¸ller, F. Bechstedt, H. Lu, and W. J. Schaff, "Anisotropy of the dielectric function for wurtzite InN," Superlattices and Microstructures **36** (4-6), pp.591-597 (2004).

[6] M. Higashiwaki and T. Matsui, "Estimation of band-gap energy of intrinsic InN from photoluminescence properties of undoped and Si-doped InN films grown by plasma-assisted molecular-beam epitaxy," J. Cryst, Growth 269(1) pp.162-166 (2004).

[7] V. P. Makhniy, M. M. Slyotov, V. V. Gorley, P. P. Horley, Yu V. Vorobiev, and J. González-Hernández, "Band structure investigations of GaN films using modulation spectroscopy," Appl. Surf. Sci. 253(1) pp.246-248 (2006).

[8] V. Kachkanov, K. P. O'Donnell, S. Pereira, and R. W. Martin, "Localization of excitation in InGaN epilayers," Phil. Mag. **87**(13) pp.1999-2017 (2007).

[9] Joseph L. Birman, "Simplified LCAO Method for Zincblende, Wurtzite, and Mixed Crystal Structures," Phys. Rev. J1 - PR **115** (6) pp.1493–1505 (1959).

[10] H. Morkoc, "Nitride Semiconductors and Devices," Springer Series in Materials Science, Vol. 32, Springer, Berlin (1999).

[11] V.Yu. Davydov, A.A. Klochikhin, R.P. Seisyan, V.V. Emtsev, S.V. Ivanov, F. Bechstedt, J. Furthmüller, H. Harima, A.V. Mudryi, J. Aderhold, O. Semchinova, J. Graul, "Absorption and Emission of Hexagonal InN. Evidence of Narrow Fundamental Band Gap," Phys. Stat. Sol. B, **229**(3) pp. r1-r3 (2002).

[12] T. Suzuki, H. Yaguchi, H. Okumura, Y. Ishida, and S. Yoshida, "Optical Constants of Cubic GaN, AlN, and AlGaN Alloys, " Jpn. J. Appl. Phys. Part 2 39, L497 (2000).

[13] Su-Huai Wei and Alex Zunger, "Giant and Composition-Dependent Optical Bowing Coefficient in GaAsN Alloys," Phys. Rev. Lett.**76**(4) pp. 664–667 (1996).

[14] M. D. McCluskey, C. G. Van de Walle, C. P. Master, L. T. Romano, and N. M. Johnson, "Large band gap bowing of $In_xGa_{1-x}N$ alloys," Appl. Phys. Lett. **72**(21) pp.2725-2726 (1998).

[15] C. A. Parker, J. C. Roberts, S. M. Bedair, M. J. Reed, S. X. Liu, N. A. El-Masry, and L. H. Robins, "Optical band gap dependence on composition and thickness of $In_xGa_{1-x}N$ ($0 < x < 0.25$) grown on GaN," Appl. Phys. Lett. 75(150 pp.2566-2568 (1999).

[16] C. Wetzel, T. Takeuchi, S. Yamaguchi, H. Katoh, H. Amano, and I. Akasaki, "Optical band gap in $Ga_{1-x}In_xN$ ($0 < x < 0.2$) on GaN by photoreflection spectroscopy," Appl. Phys. Lett. **73**(14) pp.1994-1996 (1998).

[17] H. P. D. Schenk, P. de Mierry, M. Laugt, F. Omnes, M. Leroux, B. Beaumont, and P. Gibart, "Indium incorporation above 800 °C during metalorganic vapor phase epitaxy of InGaN," Appl. Phys. Lett. **75**(17) pp. 2587-2589 (1999).

[18] R. Goldhahn, J. Scheiner, S. Shokhovets, T. Frey, U. Kohler, D. J. As, and K. Lischka, "Refractive index and gap energy of cubic $In_xGa_{1-x}N$," Appl. Phys. Lett. 76(3) pp.291-293 (2000).

[19] K. P. O'Donnell, R. W. Martin, C. Trager-Cowan, M. E. White, K. Esona, C. Deatcher, P. G. Middleton, K. Jacobs, W. Van der Stricht, C. Merlet, B. Gil, A. Vantomme, and J. F. W. Mosselmans, "The dependence of the optical energies on InGaN composition," Mat. Sci. and Eng. B **82(**1-3) pp.194-196 (2001).

[20] A. Gokarna, A. Gauthier-Brun, W. Liu, Y. Androussi, E. Dumont, E. Dogheche, J. H. Teng, S. J. Chua, and D. Decoster, "Optical and microstructural properties versus indium

content in In[sub x]Ga[sub 1 - x]N films grown by metal organic chemical vapor deposition," Appl. Phys. Lett. 96(19) pp.191909-3 (2010).

[21] Y.-H. Cho, G. H. Gainer, A. J. Fischer, J. J. Song, S. Keller, U. K. Mishra, and S. P. DenBaars, "S-shaped' temperature-dependent emission shift and carrier dynamics in InGaN/GaN multiple quantum wells," Appl. Phys. Lett. 73(10) pp. 1370-1372 (1998).

[22] Y. P. Varshni, "Temperature dependence of the energy gap in semiconductors," Physica **34**(1) pp.149-154 (1967).

[23] C. Hums, "Optische Eigenschaften von InGaN-Heterostructuren," Diplomarbeit, TU-Berlin (2004).

[24] A. K. Viswanath, J. I. Lee, C. R. Lee, J. Y. Leem, and D. Kim, "Free exciton transitions and varshni's coefficients for GaN epitaxial layers grown by horizontal lp-mocvd," Solid State Com. **108**(7), pp.483-487 (1998).

[25] F. Möglich and R. Rompe, "Über den Einfluß der Wärmedehnung auf das Absorptionsspektrum von Isolatoren," Zeitschrift für Physik A 119(7-8) pp.472-481 (1942).

[26] J. Bardeen and W. Shockley, "Deformation Potentials and Mobilities in Non-Polar Crystals," Phys. Rev. **80**(1) pp.72–80 (1950).

[27] A. B. Djurisic and E. Herbert Li, "Modeling the optical constants of hexagonal GaN, InN, and AlN," J. Appl. Phys. **85**(5) pp. 2848-2853 (1999).

[28] S. Logothetidis, J. Petalas, M. Cardona, and T. D. Moustakas, "Optical properties and temperature dependence of the interband transitions of cubic and hexagonal GaN," Phys. Rev.B **50**(24) pp.18017–18029 (1994).

[29] G. Yu, G. Wang, H. Ishikawa, M. Umeno, T. Soga, T. Egawa, J. Watanabe, and T. Jimbo, "Optical properties of wurtzite structure GaN on sapphire around fundamental absorption edge (0.78--4.77 eV) by spectroscopic ellipsometry and the optical transmission method," Appl. Phys. Lett. **70**(24) pp.3209-3211 (1997).

[30] J. Petalas, S. Logothetidis, S. Boultadakis, M. Alouani, and J. M. Wills, "Optical and electronic-structure study of cubic and hexagonal GaN thin films," Phys. Rev. B **52**(11) pp.8082–8091 (1995).

[31] T. Kawashima, H. Yoshikawa, S. Adachi, S. Fuke, and K. Ohtsuka, "Optical properties of hexagonal GaN," J. Appl. Phys. **82**(7) pp.3528-3535 (1997).

[32] A. B. Djurisic and E. H. Li, "Modeling the optical properties of hexagonal GaN," Appl. Phys. Lett. **73**(7), pp. 868-870 (1998).

[33] K. Takeuchi, S. Adachi, and K. Ohtsuka, "Optical properties of Al[sub x]Ga[sub 1 - x]N alloy," J. Appl. Phys. 107 (2),pp. 023306-023311 (2010).

[34] V.G. Dmitriev, G.G. Gurzadyan, and D.N. Nikogosyan, "Handbook of Nonlinear Optical Crystals," Springer Series in Optical Sciences. Eds.: A.L. Schawlow, K. Shimoda, A.E. Siegman, T. Tamir. Vol. 64, ISBN 3-540-61275-0, New York (1996).

[35] R.M.A. Azzam and N.M. Bashara, "Ellipsometry and Polarized Light", North-Holland, AC Amsterdam, ISBN 0-444-87016-4 (1987).

[36] O. S. Heavens, "Optical Properties of Thin Solid Films," ISBN 0-486-66924-6 , Dover Publications Inc., (1991).

[37] R. Goldhahn, P. Schley, M. Röppischer, 'Ellipsometry of InN and related alloys' in: Indium Nitride and Related Alloys, ed. by T.D. Veal, C.F. McConville, and W.J. Schaff, CRC Press ISBN: 978-1-4200-7809-1 (Boca Raton), pp. 315-375 (2009).

Appendix

Transmission calculation Program using MDF and multilayer stack approach

```
eps0=1;            %epsilon of the ambient
ds=400e-6;         %the thickness of the sappire
GaNepsinf=5;       %epsilon infinity of GaN
AG = 41.251;       %the ocillator strength of the first ocillater
E0G=3.62;          %critical point of E0
gam01G=0.287;      %broadening parameter of the first ocillator
A0exG = 0.249;     %the ocillator strength of the second ocillater (exiton contribution around
E0)
G03dG=0.03;        %binding energy of the exiton
gam1G =[0.743;0.428;0.44];     %broadening parameters for the third ocillator  include three
critical points E1G(1:3)
E1G =[6.01;8.182;8.761];       %values of the three critical points
B1G=[0.778;0.103;0.92];        %ocillator strength of the third ocilator
B1xG =[2.042;1.024;1.997];     %the ocillator strength of the fourth ocillater (exiton
contribution around three critical points E1G)
G12dG=[0.0003;0.356;1.962];    %binding energy of the exiton around three critical points E1G
alp0G=2.241;                   %a constant in Gaussian broadening


% five additional ocillator to make the calculation fit with the experiment data (not from
literature)
% s is ocillator strength, E is the position of the ocillator, gam is the
% broadening parameter of the ocillator

sab4=0.2;
Eab4=2.7;
gamab4=0.8;

sab3=0.22;
Eab3=2.3;
gamab3=0.8;


sab1=0.7;
Eab1=1.67;
gamab1=0.9;

sab5=0.3;
Eab5=1.2;
gamab5=0.8;

sab2=1.4;
```

```
Eab2=0.5;
gamab2=0.5;

A0exI = 0.001;
G03dI=0.024;

%Sellmeier Equation form Dimitriev et al. "Handbook Of Nonlinear Optical
%Chrystals" Springer 1999, p.81
%Constants are from I.H.Malitson "Refraction And Dispersion Of Synthetic
%Sapphire" J.Opt.Soc.Am.55, 1205 - 1209 (1965)
Asapphire = 1.0237980;
Bsapphire = 0.0037759;
Csapphire = 1.0582640;
Dsapphire = 0.0122544;
Esapphire = 5.2807920;
Fsapphire = 321.36160;

dg=9e-007;
data=load('509LS.dat');
d11=data(:,1);
d22=data(:,2);
llp=size(d11);
lp=llp(1);

TT=zeros(1,lp);
x=zeros(1,lp);
k=0;
GaNeps=zeros(1,lp);
Sapeps=zeros(1,lp);
dd=zeros(2,lp);
GaNi=zeros(1,lp);
GaNr=zeros(1,lp);

for wl=304:2:1700,
   k=k+1;

   E=1239.8/wl;
   x(k)=wl;
   l=wl*1e-9;


   %GaN dielectric function

   gam0G=gam01G*exp(-alp0G*(((E-E0G)/gam01G)^2));
   X0G=(E+1i*gam0G)/E0G;
   GaNeps0=AG*(E0G^(-1.5))*X0G^(-2)*(2-sqrt(1+X0G)-sqrt(1-X0G));
```

```
GaNeps0x=0;
for m = 1 :100,
   GaNeps0x = GaNeps0x + (A0exG/(m^3*E0G - m*G03dG - m^3*E - m^3*1i*gam0G));
end

GaNeps1=0;
X1G = [(E + 1i * gam1G(1))/E1G(1); (E + 1i * gam1G(2))/E1G(2) ;(E + 1i *
gam1G(3))/E1G(3)];
for m = 1 : 3,
   GaNeps1 = GaNeps1 + (B1G(m)*X1G(m)^(-2)*log(1-X1G(m)^2));
end
GaNeps1 = -1 * GaNeps1;

GaNeps1x=0;
for m = 1 : 3,
   sum = 0;
   for n = 1 : 100,
      sum = sum + (B1xG(m)/(((2*n-1)^3)*(E1G(m)-(G12dG(m)/((2*n-1)^2))-E-
1i*gam1G(m))));
   end
   GaNeps1x = GaNeps1x + sum;
end

GaNepso1=sab1/((Eab1^2-E^2)-1i*E*gamab1);
GaNepso2=sab2/((Eab2^2-E^2)-1i*E*gamab2);
GaNepso3=sab3/((Eab3^2-E^2)-1i*E*gamab3);
GaNepso4=sab4/((Eab4^2-E^2)-1i*E*gamab4);
GaNepso5=sab5/((Eab5^2-E^2)-1i*E*gamab5);

GaNepsf =
GaNeps0+GaNeps0x+GaNeps1+GaNeps1x+GaNepsinf+GaNepso1+GaNepso2+GaNepso3+Ga
Nepso4+GaNepso5;
GaNeps(k)=conj(GaNepsf);

ls=l*1000;
Sapeps(k)=1 + (Asapphire*(ls^2)/(ls^2-Bsapphire)) + (Csapphire*(ls^2)/(ls^2-Dsapphire)) +
(Esapphire*(ls^2)/(ls^2-Fsapphire));


ps1=(2*pi*dg*sqrt(GaNeps(k)))/l;
ps2=(2*pi*ds*sqrt(Sapeps(k)))/l;
%unpolarized light rp, rs are the same.

r01=(sqrt(eps0)-sqrt(GaNeps(k)))/(sqrt(eps0)+sqrt(GaNeps(k)));
r12=(sqrt(GaNeps(k))-sqrt(Sapeps(k)))/(sqrt(GaNeps(k))+sqrt(Sapeps(k)));
```

```
    r23=(sqrt(Sapeps(k))-sqrt(eps0))/(sqrt(eps0)+sqrt(Sapeps(k)));

    t01=2*sqrt(eps0)/(sqrt(eps0)+sqrt(GaNeps(k)));
    t12=2*sqrt(GaNeps(k))/(sqrt(GaNeps(k))+sqrt(Sapeps(k)));
    t23=2*sqrt(Sapeps(k))/(sqrt(Sapeps(k))+sqrt(eps0));

    t1=t01;
    t2=t12*exp(-1i*ps1);
    t3=t23*exp(-1i*ps2);


    m1=[1 r01;r01 1];
    m2=[1 r12;r12*exp(-1i*2*(ps1)) exp(-1i*2*ps1)];
    m3=[1 r23;r23*exp(-1i*2*(ps2)) exp(-1i*2*ps2)];

    M=m1*m2*m3;
    a=M(1,1);

    tt=t1*t2*t3/a;
    TT(k)=tt*conj(tt);
    InNi(k)=-imag(InNeps(k));
    InNr(k)=real(InNeps(k));
    GaNi(k)=-imag(GaNeps(k));
    GaNr(k)=real(GaNeps(k));
end

plot(x,TT,x,d22);

dd(:,1)=d11;
dd(:,2)=TT;
xlswrite('fit509LS.xls', dd);
```